Biogeosciences, 21, 5561–5589, 2024
https://doi.org/10.5194/bg-21-5561-2024

Biogeosciences Open Access EGU

Research article

Ocean acidification trends and carbonate system dynamics across the North Atlantic subpolar gyre water masses during 2009–2019

David Curbelo-Hernández[1], **Fiz F. Pérez**[2], **Melchor González-Dávila**[1], **Sergey V. Gladyshev**[3], **Aridane G. González**[1], **David González-Santana**[1], **Antón Velo**[2], **Alexey Sokov**[3], **and J. Magdalena Santana-Casiano**[1]

[1]Instituto de Oceanografía y Cambio Global (IOCAG), Universidad de Las Palmas de Gran Canaria (ULPGC), Las Palmas de Gran Canaria, Spain
[2]Instituto de Investigaciones Marinas (IIM), CSIC, Vigo, Spain
[3]P. P. Shirshov Institute of Oceanology, Russian Academy of Sciences, Moscow, Russian Federation

Correspondence: Melchor González-Dávila (melchor.gonzalez@ulpgc.es)

Received: 9 May 2024 – Discussion started: 11 June 2024
Revised: 24 September 2024 – Accepted: 30 October 2024 – Published: 13 December 2024

Abstract. The CO_2–carbonate system dynamics in the North Atlantic subpolar gyre (NASPG) were evaluated between 2009 and 2019. Data were collected aboard eight summer cruises through the Climate and Ocean: Variability, Predictability and Change (CLIVAR) 59.5° N section. The ocean acidification (OA) patterns and the reduction in the saturation state of calcite (Ω_{Ca}) and aragonite (Ω_{Arag}) in response to the increasing anthropogenic CO_2 (C_{ant}) were assessed within the Irminger, Iceland, and Rockall basins during a poorly assessed decade in which the physical patterns reversed in comparison with previous well-known periods. The observed cooling, freshening, and enhanced ventilation increased the interannual rate of accumulation of C_{ant} in the interior ocean by 50 %–86 % and the OA rates by close to 10 %. The OA trends were 0.0013–0.0032 units yr^{-1} in the Irminger and Iceland basins and 0.0006–0.0024 units yr^{-1} in the Rockall Trough, causing a decline in Ω_{Ca} and Ω_{Arag} of 0.004–0.021 and 0.003–0.0013 units yr^{-1}, respectively. The C_{ant}-driven rise in total inorganic carbon (C_T) was the main driver of the OA (contributed by 53 %–68 % in upper layers and > 82 % toward the interior ocean) and the reduction in Ω_{Ca} and Ω_{Arag} (> 64 %). The transient decrease in temperature, salinity, and A_T collectively counteracts the C_T-driven acidification by 45 %–85 % in the upper layers and in the shallow Rockall Trough and by < 10 % in the interior ocean. The present investigation reports the acceleration of the OA within the NASPG and expands knowledge about the future state of the ocean.

Key points.

- During the 2010s, the subpolar North Atlantic experienced a 50 %–86 % increase in anthropogenic CO_2, accelerating by 7 %–10 % the acidification.
- Anthropogenic CO_2 contributed to acidification by 53 %–68 % in upper layers and > 82 % in the interior ocean.
- The acidification trends (0.0006 and 0.0032 units yr^{-1}) declined the Ω_{Ca} and Ω_{Arag} by 0.004–0.021 and 0.003–0.0013 units yr^{-1}, respectively.

1 Introduction

The ocean uptake of approximately one-third of the CO_2 released into the atmosphere (Friedlingstein et al., 2023; Gruber et al., 2019) has an important role in climate regulation, causing changes in marine carbonate chemistry. The exponential increase in the global ocean CO_2 sink in phase with that of anthropogenic emissions (Friedlingstein et al., 2023) has resulted in a long-term decrease in the concentration of carbonate ions ($[CO_3^{2-}]$) and pH. This process has been collectively referred to as ocean acidification (OA; Caldeira and Wickett, 2003, 2005; Doney et al., 2009; Orr et al., 2005; Raven et al., 2005; Feely et al., 2009) and favours the dissolution of calcium carbonate ($CaCO_3$). It affects not only calcifying marine organisms and ecosystems which use the biogenic $CaCO_3$ forms of calcite and aragonite (e.g. Gattuso et al., 2015; Langdon et al., 2000; Pörtner et al., 2004, 2019; Riebesell et al., 2000) but also the global biogeochemical cycles (Gehlen et al., 2011; Matear and Lenton, 2014).

Published by Copernicus Publications on behalf of the European Geosciences Union.

The absorption of anthropogenic CO_2 has reduced the pH of the global surface ocean by 0.1 units since preindustrial times, representing an approximately 30 % increase in acidity (Caldeira and Wickett, 2003). According to the IPCC's Representative Concentration Pathway (RCP) scenarios (Van Vuuren et al., 2011; Moss et al., 2010), which project various future trajectories of greenhouse gas concentrations, the model projections estimate a potential pH decrease of 0.3–0.4 units by the end of the century under the RCP8.5 scenario, which assumes continued high CO_2 emissions. In contrast, the most conservative RCP2.6 scenario, which includes significant emission reductions, anticipates a pH drop of 0.2–0.3 units (IPCC, 2013, 2021). However, as the absorption and storing of anthropogenic carbon (C_{ant}), defined as the fraction of inorganic carbon resulting from human emissions (Sarmiento et al., 1992), is not uniform within the ocean (Sabine et al., 2004), OA rates may show a significant spatial variability and should be studied regionally. The temporal evolution of the carbonate system variables in surface waters are monitored and assessed in several time series stations located across different ocean regions (Bates et al., 2014). The largest OA rates are expected to occur across high northern and southern latitudes (Bellerby et al., 2005; Orr et al., 2005), where deep convective overturning and subduction occur, favouring the entrance of C_{ant} in the interior ocean (Maier-Reimer and Hasselmann, 1987; Lazier et al., 2002; Sarmiento et al., 1992).

The North Atlantic is one of the strongest CO_2 sinks and stores over 25 % of the C_{ant} accumulated in the global ocean (e.g. Gruber et al., 2019; Khatiwala et al., 2013; Pérez et al., 2008, 2010, 2024; Sabine et al., 2004; Takahashi et al., 2009). The Atlantic Meridional Overturning Circulation (AMOC) plays a significant role by conveying acidified C_{ant}-loaded waters polewards and exporting them to the ocean interior across deep-water formation areas (Lazier et al., 2002; Pérez et al., 2008, 2013; Steinfeldt et al., 2009). It contributes to homogenizing the C_{ant} and pH in the whole water column in such regions and exports these properties southwards to the global deep ocean (Pérez et al., 2018). Thus, the North Atlantic behaves as a crucial region for understanding the impacts of anthropogenic forcing on the global ocean.

OA has been widely studied in the North Atlantic through the monitoring of the ocean physicochemical properties at time series stations (summarized by Bates et al., 2014) placed in subtropical and subpolar latitudes: the European Station for Time-Series in the Ocean of the Canary Islands (ESTOC; 29.04° N, 15.50° W; González-Dávila et al., 2010; González-Dávila and Santana-Casiano, 2023; Santana-Casiano et al., 2007), the Bermuda Atlantic Time-series Study (BATS; 32.0° N, 64.0° W; Bates et al., 2012), the Irminger Sea time series (IRM-TS; 64.3° N, 28.0° W; Olafsson et al., 2010), and the Iceland Sea time series (IS-TS; 68.0° N, 12.66° W; Olafsson et al., 2009, 2010). OA rates have also been evaluated along transects through repeated hydrographic cruises (i.e. Guallart et al., 2015; García-Ibáñez et al., 2016; Vázquez-Rodríguez et al., 2012b) or even covered by volunteer observing ships (Fröb et al., 2019). These investigations have revealed a rate of decrease in pH of ~ 0.001–0.002 units yr^{-1}. Moreover, González-Dávila and Santana-Casiano (2023) recently indicated that these rates have been increasing since 1995.

The assessment of OA is of special interest across the North Atlantic subpolar gyre (NASPG; 50–60° N), where the atmospheric CO_2 sink is particularly strong and the deep-water formation processes favour the storage of C_{ant} through the whole water column (Gruber et al., 2019; Sabine et al., 2004; Watson et al., 2009; Pérez et al. 2008). Likewise, the deep-water formation processes create the largest and deepest ocean environments supersaturated for aragonite (at more than 2000 m depth; Feely et al., 2004; Jiang et al., 2015), which is the main $CaCO_3$ mineral for cold-water corals (CWCs; Roberts et al., 2009) and some pteropods (Bathmann et al., 1991; Urban-Rich et al., 2001). These deep biomes are predicted to be among the first in the global ocean affected by OA, mainly due to the shoaling of the aragonite saturation horizon and its progressive exposition to undersaturated conditions for aragonite at intermediate and deep waters (Gehlen et al., 2014; Guinotte et al., 2006; Raven et al., 2005; Roberts et al., 2009; Turley et al., 2007).

The physical processes along the NASPG, which are subject to significant spatiotemporal variability introduced by the atmospheric forcing and climatology on an interannual scale, directly influenced the biogeochemistry (Corbière et al., 2007; Fröb et al., 2019). The changes in the North Atlantic Current (NAC) modify the poleward heat transport from subtropical latitudes and air–sea interactions, influencing temperature patterns (Josey et al., 2018; Mercier et al., 2015). Recent studies noticed the surface cooling and freshening of the NASPG in the 2010s (Holliday et al., 2020; Josey et al., 2018; Robson et al., 2016; Tesdal et al., 2018) contrasting with the period of warming and salinification in the 1990s extended until 2005 (Häkkinen and Rhines, 2004; Hátún et al., 2005; Robson et al., 2014). Anomalous heat loss and winter deep convection were found to be of high intensity since 2008, contributing to the extreme cold anomaly along the NASPG (e.g. de Jong et al., 2012; de Jong and de Steur, 2016; Fröb et al., 2019, 2016; Gladyshev et al., 2016a, b; Piron et al., 2017; Våge et al., 2009). These fluctuations in the vertical mixing and ocean circulation patterns introduce changes in the distribution of the carbonate system variables.

The estimated OA trend over 1991–2011 for surface waters across the North Atlantic subpolar biome was -0.0020 ± 0.0001 units yr^{-1} (Lauvset et al., 2015). Chau et al. (2024) recently reported that the surface waters in the Irminger and Iceland basins acidified over 1985–2021 at rates of -0.0016 ± 0.0001 and -0.0014 ± 0.0001 units yr^{-1}. Several observation-based investigations have evaluated the drivers, trends, and impacts of OA through the entire water column in the Irminger and Iceland basins (e.g. Fontela et al., 2020; García-Ibáñez et al., 2016, 2021; Perez et al., 2018;

Pérez et al., 2021; Ríos et al., 2015), while few studies have addressed it in the Rockall Trough (e.g. McGrath et al., 2013, 2012a, b; Humphreys et al., 2016) due to the lack of repeated hydrographic sections or time series stations and the subsequent limitation of continuous surface-to-bottom data. The high longitudinal variability in the NASPG caused by the influence of different circulation patterns and water masses (García-Ibáñez et al., 2015, 2018) introduced several physicochemical heterogeneities between the Irminger and Iceland basins and the Rockall basin (Ellett et al., 1986; McGrath et al., 2013, 2012b; Holliday et al., 2000). These differences in the distributions of marine carbonate system (MCS) variables should be considered to improve our understanding of OA in the entire North Atlantic.

This study evaluated the OA in the NASPG across the Irminger, Iceland, and Rockall basins during the 2010s. High-quality direct measurements of CO_2 system variables from eight hydrographic cruises occupying 59.5° N between 2009 and 2019 were used to evaluate the drivers and trends of pH and the potential effects of OA on calcifying organisms of changes in calcite (ΩCa) and aragonite (ΩAr) saturation states. This study advances our understanding of the complexities associated with OA in the NASPG and supports ongoing efforts to model and predict future acidification scenarios in the North Atlantic and global ocean.

2 Methodology

2.1 Data collection

Data were collected from eight summer cruises conducted along the transverse hydrographic section at 59.5° N between 2009 and 2019 (Daniault et al., 2016; Gladyshev et al., 2016b, 2017, 2018; Sarafanov et al., 2018). This section is part of the World Climate Research Programme (WCRP) within the framework of the Climate and Ocean: Variability, Predictability and Change (CLIVAR) project and covers the length of the subpolar North Atlantic between Scotland and Greenland (4.5–43.0° W), crossing the Irminger and Iceland basins and the Rockall Trough (Fig. 1). Generally, the sampling stations were equidistantly spaced every 20 nmi ($\sim 1/3°$ longitude), and this was repeated in all the cruises except for the cruise of 2016, when the station spacing was decreased to 10 nmi over the Reykjanes Ridge western and eastern slopes. The distance between stations over the eastern Greenland slope and shelf always decreased from 10 nmi to about 2 nmi. The surface-to-bottom sampling and in situ measurements were performed by using an SBE 911plus CTD with an SBE32 Carousel containing 24 Niskin bottles (10 L) with additional sensors for pressure (P), dual temperature (T), salinity (S), and dissolved oxygen (DO). The eight cruises included in the new dataset are the result of an international collaboration between researchers from the P. P. Shirshov Institute of Oceanology at the Russian Academy of Science and the Marine Chemistry research group from the Oceanography and Global Change Institute (QUIMA-IOCAG) at the University of Las Palmas de Gran Canaria (ULPGC). A detailed overview of the cruises is given in Table 1.

2.1.1 CO_2 system variable measurements

The analysis of the MCS variables followed the same analytical methodology and provided high-quality CO_2 measurements on all the hydrographic cruises. This includes the sampling and data collection techniques and the quality control and calculation procedures published in the updated version of the DOE method manual for CO_2 analysis in seawater given by Dickson et al. (2007). The seawater samples were analysed on board for total alkalinity (A_T) and total inorganic carbon (C_T) determination by using a VINDTA 3C and following Mintrop et al. (2000). The A_T was analysed by potentiometric titration with HCl to the carbonic acid endpoint and determined through the development of the full titration curve (Millero et al., 1993; Dickson and Goyet, 1994). The C_T was determined through coulometric titration (Johnson et al., 1993). The VINDTA 3C was calibrated through the titration of certified reference materials (CRMs; provided by Andrew Dickson at the Scripps Institution of Oceanography), giving values with an accuracy of $\pm 1.5\,\mu mol\,kg^{-1}$ for A_T and $\pm 1.0\,\mu mol\,kg^{-1}$ for C_T.

Spectrophotometric pH measurements (Clayton and Byrne, 1993) in total scale at a constant temperature of 15 °C ($pH_{T,15}$) were performed for the cruises between 2009 and 2016. A spectrophotometric pH sensor (SP101-SM) developed by the QUIMA-IOCAG group at the ULPGC in collaboration with SensorLab (González-Dávila et al., 2014, 2016) was used. The method uses four wavelength analyses for pH indicator dyes (*m*-cresol purple), includes auto-cleaning steps, and performs a blank for pH calculation immediately after the dye injection. The spectrophotometric sensor was in situ tested by using a Tris seawater buffer (Ramette et al., 1977) and provided $pH_{T,15}$ values with an accuracy of ± 0.002 units. To account for the systematic uncertainty reported by DelValls and Dickson (1998) related to the pK* values of *m*-cresol purple, and in line with their recommendations, a correction of $+0.0047$ units was applied to the measured $pH_{T,15}$. This adjustment ensures that the calculated pH values are consistent with the more accurate pK* determinations.

2.1.2 Dissolved oxygen (DO) measurements

The Winkler method introduced by Winkler (1888) and optimized by Carpenter (1965) and Carrit and Carpenter (1966) was used to analytically determine the dissolved oxygen (DO) of the seawater samples in all the cruises from 2009–2016. The seawater samples for DO determination were collected from the bottle samples in pre-calibrated wide-

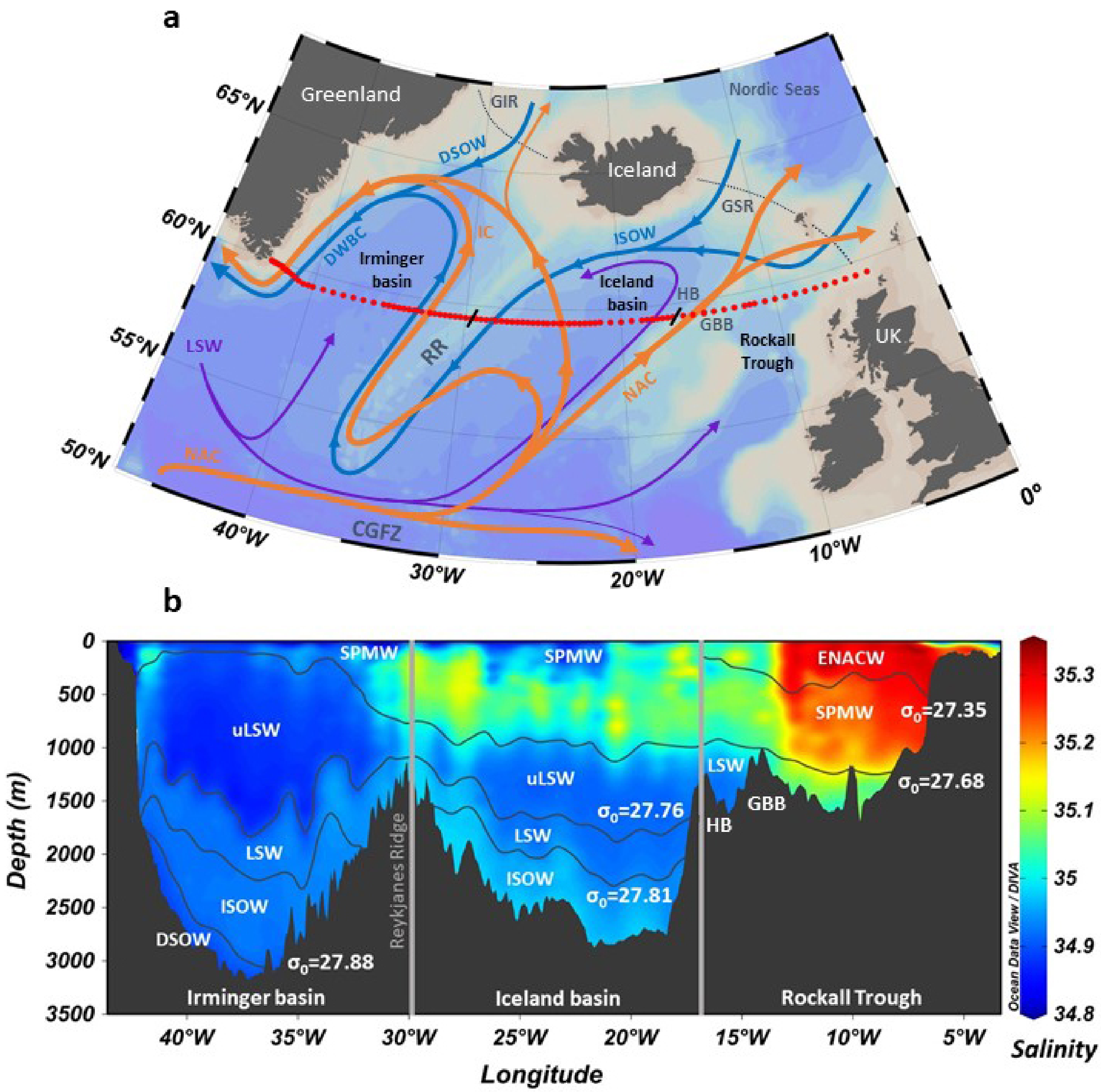

Figure 1. (a) Map of the North Atlantic subpolar gyre (NASPG) with the schematic diagram of the surface and deep circulation patterns compiled from Lherminier et al. (2010), Pérez et al. (2021), Sarafanov et al. (2012), Schmitz and McCartney (1993), Schott and Brandt (2007), and Sutherland and Pickart (2008). The acronyms are defined as follows: the bathymetric features are shown in grey (RR: Reykjanes Ridge; HB: Hatton Bank; GBB: George Bligh Bank; CGFZ: Charlie–Gibbs Fracture Zone; GIR: Greenland–Iceland Ridge; and GSR: Greenland–Scotland Ridge), the surface currents are shown in orange (NAC: North Atlantic Current; IC: Irminger Current), and the deep-water circulation is shown in blue and purple (ISOW: Iceland–Scotland Overflow Water; DSOW: Denmark Strait Overflow Water; LSW: Labrador Sea Water; and DWBC: Deep Western Boundary Current). The longitudinal distribution of the surface-to-bottom sampling stations along the cruise track of 2016 (repeated throughout the cruises) is shown with red dots. The black lines along the cruise track delimit the three basins. **(b)** Vertical distribution of the water masses considered in this study for each of the basins. The isopycnals, plotted over the salinity distribution for the cruise of 2016, show the limits of the layers and were defined by potential density (in $\mathrm{kg\,m^{-3}}$) referred to 0 dbar (σ_0). The vertical grey lines show the limits between basins. The water masses (ENACW: eastern North Atlantic Central Water; SPMW: Subpolar Mode Water; uLSW: upper Labrador Sea Water; LSW: Labrador Sea Water; ISOW: Iceland–Scotland Overflow Water; DSOW: Denmark Strait Overflow Water) and the selection of potential density values delimiting the layers are described in Sect. 2.2.4. Figure produced with Ocean Data View (Schlitzer, Reiner, Ocean Data View, https://odv.awi.de, last access: 9 December 2024, 2021).

Table 1. Metadata list of hydrographic cruises.

Year	Cruise ID	Date	*Research Vessel* (R/V)	Chief Scientist	Number of stations	MCS measured variables
2009	AI28	15 Aug–27 Sept	Akademik Ioffe	A. Sokov	67	A_T, C_T, and pH
2010	AI31	2–27 Sep	Akademik Ioffe	A. Sokov	84	A_T, C_T, and pH
2011	SV33	9–28 Sep	Akademik Sergey Vavilov	A. Sokov	98	A_T, C_T, and pH
2012	AI38	25 May–1 Jul	Akademik Ioffe	S. Gladyshev	66	A_T, C_T, and pH
2013	AI41	26 Jun–23 Jul	Akademik Ioffe	S. Gladyshev	75	A_T, C_T, and pH
2014	AI44	27 Jun–20 Jul	Akademik Ioffe	S. Gladyshev	76	A_T, C_T, and pH
2016	AI51	3 Jun–13 Jul	Akademik Ioffe	S. Gladyshev	104	A_T, C_T, and pH
2019	AMK77	8 Aug–10 Sep	Akademik Mstislav Keldysh	S. Gladyshev	47	A_T and C_T

neck glass bottles, avoiding bubble formation. The temperature of the water was recorded during the sampling. All the reagents and solutions used for dissolved oxygen determination were prepared following the procedures described by Dickson (1995), and their possible impurities were controlled by determining a blank every 2 d.

As DO could not be analytically measured during the cruise of 2019 (due to limitations related to the oceanographic cruise plan), it was computed for this year by comparing the performance of the DO sensor during the cruise of 2019 versus (1) DO data estimated by a neural network for the cruises of 2016 and 2019 and (2) Winkler-measured DO data during the cruise of 2016. The neural network ESPER_NN (Empirical Seawater Property Estimation Routine) introduced by Carter et al. (2021) was used for DO estimations. The computational procedure is detailed in Appendix A.

2.2 Data processing

2.2.1 Evaluation of the internal consistency of the data using CANYON-B

The measured and determined data were compared with estimations given by the Bayesian neural network "CANYON-B" (Bittig et al., 2018), a re-developed and more robust neural network based on CANYON (CArbonate system and Nutrients concentration from hYdrological properties and Oxygen using a Neural-network; Sauzède et al., 2017). CANYON-B estimates the four MCS variables (A_T, C_T, pH, and $p\mathrm{CO_2}$) and macronutrient concentrations (PO_4^{3-}, NO_3^-, and $Si(OH)_4$, hereinafter PO_4, NO_3, and $Si(OH)_4$) as a function of a simple set of input variables which include P, T, S, DO, latitude, longitude, and date. This neural network is trained on and validated against bottle data from GLODAPv2 and recent GO-SHIP profiles and compared with sensor data from Argo floats. The standard errors of estimation reported for CANYON-B by Bittig et al. (2018) are 6.3 µmol kg^{-1} for A_T, 7.1 µmol kg^{-1} for C_T, 0.013 units for pH, 20 µatm for $p\mathrm{CO_2}$, 0.051 µmol kg^{-1} for PO_4, 0.68 µmol kg^{-1} for NO_3, and 2.3 µmol kg^{-1} for $Si(OH)_4$. The crossover analysis between measured and estimated data did not show systematic differences but showed individual outliers. The measured data that were higher/lower than the CANYON-B estimate by plus/minus twice the predicted variable uncertainty of the neural network were regarded as outliers and removed from the dataset.

The total number of measured data was 8974 for A_T, 7495 for C_T, 8706 for $\mathrm{pH}_{T,15}$, 9656 for DO, 9114 for PO_4, and 9192 for $Si(OH)_4$. The difference between the measured and CANYON-B-estimated variables (referred to hereinafter as canyon-estimated variables) was performed for each sample in which CANYON-B could be applied (samples with availability of T, S, and DO measurements). The number of data, mean values, and standard deviation of the measured variables for each cruise are summarized in Table S1. The average differences with the 95 % confidence interval for each cruise are shown in Table S2. The average differences for the entire period (2009–2019) were lower than 2.1 µmol kg^{-1} for A_T, 2 µmol kg^{-1} for C_T, 0.0002 for pH, 0.02 µmol kg^{-1} for PO_4, and 0.25 µmol kg^{-1} for $Si(OH)_4$. The minimal difference between the measured and the canyon-estimated pH instils confidence in the correction applied to the measured pH following DelValls and Dickson (1998).

2.2.2 Computational methods

The computational procedures to calculate MCS variables applied in this investigation used the $\mathrm{CO_{2,SYS}}$ programme developed by Lewis and Wallace (1998) and were run with the MATLAB software (van Heuven et al., 2011; Orr et al., 2018; Sharp et al., 2023). The set of constants used for computations includes the carbonic acid dissociation constants of Lueker et al. (2000), the HSO_4^- dissociation constant of Dickson (1990), the HF dissociation constant of Pérez and Fraga (1987), and the value of $[B]_T$ determined by Lee et al. (2010). The pH in total scale at in situ temperature ($\mathrm{pH_T}$) was computed from the measured A_T and $\mathrm{pH}_{T,15}$ (the computed C_T was given as an output). The $\mathrm{pH_T}$ for the cruise of 2019, in which direct pH measurements were not performed, was computed from the measured A_T and C_T.

The saturation states of calcite (Ω_{Ca}) and aragonite (Ω_{Arag}), determined from the product of the ion concentrations of calcium ($[Ca^{2+}]$) and carbonate ($[CO_3^{2-}]$) divided by the stoichiometry solubility products (K_{sp}) for calcite (K_{Ca}) and aragonite (K_{Arag}) given by Mucci (1983), were generated as outputs of the $CO_{2,SYS}$ computational routine. The decrease in Ω_{Ca} and Ω_{Arag} reports the adverse impacts of OA on marine calcification processes (e.g. Gattuso et al., 2015; Langdon et al., 2000; Pörtner et al., 2004, 2019; Riebesell et al., 2000).

An internal consistency test was conducted on the three measured MCS variables. The measured variables were compared with canyon-estimated and $CO_{2,SYS}$-computed variables. The average differences and standard deviations were summarized in Table S2 and ensure the consistency of the observations. In addition, due to gaps in data, an intercomparison between measured and computed C_T and $pH_{T,15}$ was performed. It considers the availability of measurements for each latitude, longitude, and time and the differences between the measured and computed pH with the canyon-estimated pH_T. The use of measured or computed C_T followed these conditions: (1) if there was measured C_T but not measured pH, measured C_T was used; (2) if there was measured pH but not measured C_T, computed C_T was used; (3) and if there was measured C_T and pH, measured C_T was used when the differences between measured and canyon pH_T were lower than the differences between computed and canyon-estimated pH_T, while computed C_T was used when the opposite happened. In total, 6375 measured and 2872 computed C_T data were used in this study (69 % and 31 %, respectively). The average differences on each cruise between the combined (measured and computed, also referred to as "$C_{T\,(new)}$") and canyon-estimated C_T variable are provided in Table S2. The amount and percentage of measured and computed C_T data per cruise are given in Table S3. As the measured C_T was on average 1.9 µmol kg^{-1} higher than the canyon-estimated and the computed C_T was on average 1.7 µmol kg^{-1} lower, the new compilation based on these previous conditions allowed us to reduce the difference to 1.5 µmol kg^{-1}.

2.2.3 Anthropogenic CO_2 (C_{ant}) calculation

The anthropogenic CO_2 (C_{ant}) was estimated by using the biogeochemical back-calculation $\phi C_T{}^\circ$ method, which has an overall estimated uncertainty of ± 5.2 µmol kg^{-1} (Pérez et al., 2008; Vázquez-Rodríguez et al., 2009). The method considers the change in C_T between the preindustrial era (1750) and the time of the observations, along with the processes involved in the uptake and distribution of C_{ant} (biogeochemistry, mixing processes, and air–sea fluxes). The C_{ant} was calculated (Eq. 1) as the difference between the C_T at the time of observation, the C_T that the seawater would have in equilibrium with a preindustrial atmosphere (preformed C_T, C_T^{pre}), the offsets of such equilibrium values (air–sea CO_2 disequilibrium, ΔC_T^{dis}), and the changes in C_T due to the organic and carbonate pumps (ΔC_T^{bio}). The C_T and A_T at the time of observations and the preformed A_T (A_T^0) are needed as input parameters, and the computational procedure was described by Vázquez-Rodríguez et al. (2012a).

$$C_{ant} = C_T - C_T^{pre} - \Delta C_T^{dis} - \Delta C_T^{bio} \quad (1)$$

The $\phi C_T{}^\circ$ method is an improved process-based C_{ant} estimation method tested and widely applied in the Atlantic Ocean (Vázquez-Rodríguez et al., 2009), which presents distinctive characteristics relative to existing C_{ant} approaches, such as the classical ΔC^* (GSS' 96; Gruber et al., 1996) and the TrOCA (Touratier et al., 2007). The main advantages of the $\phi C_T{}^\circ$ method were described by Pérez et al. (2008).

2.2.4 Hydrographic characterization

The characterization of the basins and water masses was done by considering the 2009–2019 mean combined 59.5° N section constructed with potential vorticity, dissolved oxygen and salinity together with the large-scale circulation in the North Atlantic (e.g. Lherminier et al., 2010; Pérez et al., 2021; Sarafanov et al., 2012; Schmitz and McCartney, 1993; Schott and Brandt, 2007; Sutherland and Pickart, 2008). A schematic diagram with the main surface and deep currents in the NASPG is depicted in Fig. 1a. The basin division considered the NAC pathways and revealed a west-to-east distribution comprising the Irminger and Iceland basins and the Rockall Trough. The Iceland basin was delimited along its eastern boundary by the central NAC branches around the northern part of the Hatton Bank and George Bligh Bank and along its western boundary by the return current over the eastern flank of the Reykjanes Ridge slope. This suggests that the Iceland basin could be longitudinally separated into two subregions: the western Iceland basin (24.0–29.5° W) and the eastern Iceland basin (14.0–24.0° W).

The upper layers were mainly occupied by Subpolar Mode Water (SPMW) and North Atlantic Central Water (NACW). SPMW is formed in the Iceland basin (McCartney and Talley, 1982; Brambilla and Talley, 2008; Tsuchiya et al., 1992; van Aken and Becker, 1996), flows eastward to the Rockall Trough, and recirculates across the Reykjanes Ridge (Brambilla and Talley, 2008). In the Irminger basin, SPMW flows with the Irminger Current to the north over the western Reykjanes Ridge flank and to the south over the eastern Greenland slope (Fig. 1a). Thus, SPMW signal was detected in the western and eastern Irminger basin up to 400–700 m depth and limited to subsurface depths in the central part of the basin. NACW was placed above SPMW east of the Irminger basin and separated into two branches: eastern North Atlantic Central Water (ENACW), formed by winter convection in the inter-gyre region and moved poleward from the Bay of Biscay through the Rockall Trough (Harvey, 1982; Pollard et al., 1996), and western North Atlantic Central Water (WNACW), flowing northward with the NAC along the western Iceland basin. The intermediate layers were mainly occupied by Labrador Sea Water (LSW), formed in the Labrador Sea and transported eastward (e.g. Pickart et al., 2003; Fröb et al., 2016). The LSW path diverges into two cores when it reaches the Reykjanes Ridge (Álvarez et al., 2004; Pickart et al., 2003): a fraction of LSW rapidly moved to the Irminger basin and incorporated into the Deep Western Boundary Current (DWBC) (Bersch et al., 2007), and a second LSW core was transported eastward into the Iceland and Rockall basins. In the Irminger and western Iceland basin, LSW placed above Iceland–Scotland Overflow Water (ISOW), which originated from the overflow of Norwegian Sea waters over the Iceland–Scotland ridges and flowed southward and below 1500 m depth through the western NASPG (van Aken and de Boer, 1995; Dickson et al., 2002; Fogelqvist et al., 2003). The bottom of the western Irminger basin was occupied by Denmark Strait Overflow Water (DSOW), recently formed from deep waters from the Nordic seas flowing southward over the Greenland–Iceland ridge and sinking through the eastern Greenland slope (Read, 2000; Stramma et al., 2004; Yashayaev and Dickson, 2008). LSW core transported eastwards rises in depth through the western Hatton Bank flank and occupies the bottom depths in the eastern Iceland basin and in the Rockall Trough. A low-ventilated thermocline layer is placed between SPMW and LSW in the eastern NASPG (García-Ibáñez et al., 2016), which represents the product of mixing with waters coming from the south (i.e. Mediterranean Waters; MW).

To enhance the comprehension of the spatial distribution and trends of the biogeochemical variables and to facilitate comparisons with previous studies along the NASPG, the hydrographic characterization was simplified based on the following principles: (1) the Iceland basin was not divided into its western and eastern parts, and its longitudinal span was delimited by the Reykjanes Ridge (29.5° W) and the Hatton Bank (17° W); (2) upper Labrador Sea Water (uLSW) was separated from deeper LSW (e.g. Stramma et al., 2004); (3) the weak and spatially limited influence of the return current and WNACW was removed by considering the upper and intermediate layers of both the Irminger basin and the Iceland basin fully occupied by SPMW above uLSW; and (4) only the eastern branch of NACW (ENACW), placed above SPMW, was contemplated for the upper Rockall Trough.

The whole water column was separated into layers delimited by potential density isopycnals at a reference pressure of 0 dbar following Azetsu-Scott et al. (2003), Kieke et al. (2007), Pérez et al. (2008), and Yashayaev et al. (2008). The vertically distributed water masses separated into density layers are represented for the entire section in Fig. 1b. The vertical characterization in density layers allows us to consistently compare the low-variable physical and chemical properties within each water mass, enabling us to assume linearity in the ocean CO_2 system. The determination of the isopycnal limits between layers in the Irminger and Iceland basins followed previous biogeochemical studies in the western boundary of the North Atlantic (Fontela et al., 2020; García-Ibáñez et al., 2016; Pérez et al., 2008, 2010; Vázquez-Rodríguez et al., 2012a). The surface-to-bottom distribution of the main water masses in these basins (with their respective σ_0 lower limits shown in brackets) was SPMW (27.68 kg m^{-3}), uLSW (27.76 kg m^{-3}), LSW (27.81 kg m^{-3}), and ISOW (27.88 kg m^{-3}). The low-temperature and low-salinity DSOW was considered at the bottom of the westernmost part of the Irminger basin. The hydrography of the Rockall Trough has been characterized in previous studies in the northeastern Atlantic (e.g. Ellett et al., 1986; Harvey, 1982; McGrath et al., 2012a, b; Holliday et al., 2000), with the main water masses surface-to-bottom distributed as ENACW (27.35 kg m^{-3}), SPMW (27.68 kg m^{-3}), and LSW (bottom).

2.2.5 Data adjustment for trend computation

The interannual trends were analysed through the whole water column across the Irminger, Iceland, and Rockall basins by yearly averaging the variables for each layer, following previous studies in the NASPG (e.g. Fontela et al., 2020; Garcììa-IbaìnÞez et al., 2016). Linear regressions were applied to the mean values, in which the value of the slope gives the ratios of interannual changes. The errors of the means were calculated through the relation of the standard deviation and the square root of the number of bottle samples in each layer and cruise (standard deviation/$\sqrt{n}$). The standard errors of the slopes were calculated by accounting for the error propagation of the annual mean values. The Pearson correlation test was employed to assess the strength and direction of the linear regressions and to evaluate the significance of the interannual trends. This test provided correlation coefficients (r^2) and corresponding p-values to determine statistical significance. The p-values ≤ 0.01 indicated that the trends were statistically significant at the 99 % confidence level, the p-values ≤ 0.05 indicated that the trends were statistically significant at the 95 % confidence level, and the p-values ≤ 0.1 indicated that the trends were statistically significant at the 90 % level. Trends with p-values > 0.1 were regarded as not statistically significant but provided an estimation of the temporal evolution of the variables in their respective layers. These not statistically significant trends were explained by the high variability and changes in the low-limit depth of the layers encountered between consecutive years.

As there was a lack of in situ measurements and sampling along the western half of the Irminger basin (36.5–42.5° W) on the cruise of 2019 (due to permit restrictions on studying the national waters of Denmark), the GO-SHIP A25-OVIDE data for the cruise of 2018 (available at SEANOE, https://www.seanoe.org/, last access: 9 December 2024; Lherminier et al., 2022) were considered to adjust the 2019 data. The average values were calculated with both the available data in the easternmost part of the Irminger basin during the cruise of 2019 and the A25-OVIDE-2018 data available in the same part of the section (29.6–36.5° W). The difference between these average values provides the variation in each variable from 2018 to 2019, which can be extrapolated to the western part of the Irminger basin by assuming linearity in the temporal evolution. Thus, the average values for 2019 were adjusted by applying the product with the calculated change between 2018 and 2019.

2.2.6 Deconvolution of the trends

OA trends arise due to the combined variations in T, S, C_T, and A_T. The influence of each driver on OA and subsequent impacts on marine calcification processes was analysed by assuming linearity and employing a first-order Taylor series deconvolution (Sarmiento and Gruber, 2006) to evaluate the trends for pH_T (Fröb et al., 2019; García-Ibáñez et al., 2016; Pérez et al., 2021; Takahashi et al., 1993; Tjiputra et al., 2014) and Ω (García-Ibáñez et al., 2021). The interannual rates of change in pH_T and Ω result from the sum of their partial derivatives versus T, S, C_T, and A_T, calculated based on the mean properties of each layer. The most recent equation defined by Pérez et al. (2021) was used (Eq. 2), in which X represents pH_T, Ω_{Ca}, and Ω_{Arag}. and salinity-normalized C_T and A_T (NC_T and NA_T, normalized to a constant salinity of 35) were used to remove the effect of the freshwater fluxes and evaporation/precipitation effects.

$$\frac{dX}{dt} = \frac{\partial X}{\partial T}\frac{dT}{dt} + \left(\frac{\partial X}{\partial S} + \frac{NC_T}{S_0}\frac{\partial X}{\partial C_T} + \frac{NA_T}{S_0}\frac{\partial X}{\partial A_T}\right)\frac{dS}{dt} + \frac{S}{S_0}\frac{\partial X}{\partial C_T}\frac{dNC_T}{dt} + \frac{S}{S_0}\frac{\partial X}{\partial A_T}\frac{dNA_T}{dt} \quad (2)$$

It is important to remark that the changes in NA_T and NC_T are linked with biogeochemical processes which have different influences: the processes involved in the organic carbon pump contribute to strongly change the NC_T weakly affecting the NA_T, while those involved in the carbonate pump affect the NA_T twice as much as NC_T. The complexity and heterogeneity of the processes that govern the pH_T change were considered by this equation.

3 Results

The vertical distribution of the physical and biogeochemical variables is depicted for the cruises of 2009 and 2016 in Figs. 2, 3, S2, and S3. The subsurface layers were characterized by warmer and saltier waters than intermediate and deep layers among the three basins (Fig. 2a and b). A west-to-east increase in temperature and salinity throughout the water column was observed in all the cruises. The temperature and salinity signals were highest in the Rockall Trough (4.5–11.0 °C and 35.0–35.4, respectively), followed by the Iceland basin (3.0–7.5 °C and 34.9–35.2, respectively) and the Irminger basin (1.5–6.5 °C and 34.8–35.1, respectively). The longitudinal differences in temperature were more remarkable toward the upper layers through the SPMW and uLSW.

The spatial variability in the physical properties introduced heterogeneities in the distribution of the CO_2 system variables. The A_T shows a well-correlated linear relationship with salinity throughout the region ($A_T = 54.57$ (± 0.36) salinity $+ 396.7$ (± 12.7); $r^2 = 0.90$ and p-value < 0.01; standard error of estimate of 2.9 µmol kg^{-1}), with lower and vertically homogenized average values in the Irminger basin (2302.8–2307.3 µmol kg^{-1} in subsurface waters and 2298.8–2301.0 µmol kg^{-1} in bottom waters) and Iceland basin (2308.7–2315.0 µmol kg^{-1} in subsurface waters and 2305.2–2308.0 µmol kg^{-1} in bottom waters) compared to the Rockall Trough (2317.9–2329.1 µmol kg^{-1} in subsurface waters and 2308.5–2310.9 µmol kg^{-1} in bottom waters).

The upper layers were characterized by low C_T values (2153.7–2160.8 µmol kg^{-1} in the Irminger basin, 2158.1–2168.4 µmol kg^{-1} in the Iceland basin, and 2120.1–2131.0 µmol kg^{-1} in the Rockall Trough), while a rapid increment with depth was found below 100–200 m depth (2154.7–2171.2 µmol kg^{-1} throughout the section). The notable difference in the distribution of A_T and C_T (Figs. 2c and 3a, respectively) compared to that of NA_T and NC_T (Fig. S2) elucidated the remarkable significance of freshwater fluxes on the carbon variable fluctuations during the period of study. The entrance of C_{ant} through the atmosphere–seawater interface caused higher C_{ant} values in the upper layers (higher than 50 µmol kg^{-1} in the first 1000 m depth; Fig. 3b). The natural component of the C_T ($C_{nat} = C_T - C_{ant}$; Fig. 3c) correlated with C_T ($r^2 = 0.87$), and showed a distribution characterized by low surface (< 2110 µmol kg^{-1}) and high bottom (> 2130 µmol kg^{-1}) concentrations.

The pH_T (Fig. 2d) rapidly decreased with depth, showing the effect of biological uptake in the upper layers and remineralization in deeper areas. The subsurface layer up to 100–200 m depth exhibited pH_T values higher than 8.025 units, which fell to 7.975 units in the bottom layers. The pH_T profiles reported an intrusion of remineralized and poorly oxygenated water between 500 and 1000 m depth with relatively low pH_T (< 7.975) compared to adjacent layers in the Iceland basin and in the western part of the Rockall Trough. This thermocline layer was previously observed at ~ 500 m depth by García-Ibáñez et al. (2016) along a more meridional transect which crossed the Iceland basin northwest–southeast. It introduces differences in the intermediate water masses between the Iceland and Rockall basins and the Irminger basin.

The spatial and interannual fluctuations in the ventilation rates through changes in the water mass formation and respiration processes represent a source of variability in the biogeochemical patterns. The apparent oxygen utilization (AOU), defined as the difference between saturated oxygen (calculated following Benson and Krause, 1984) and measured oxygen, was used to assess the ventilation of the water masses (Fig. 2e). The high AOU values indicate low ventila-

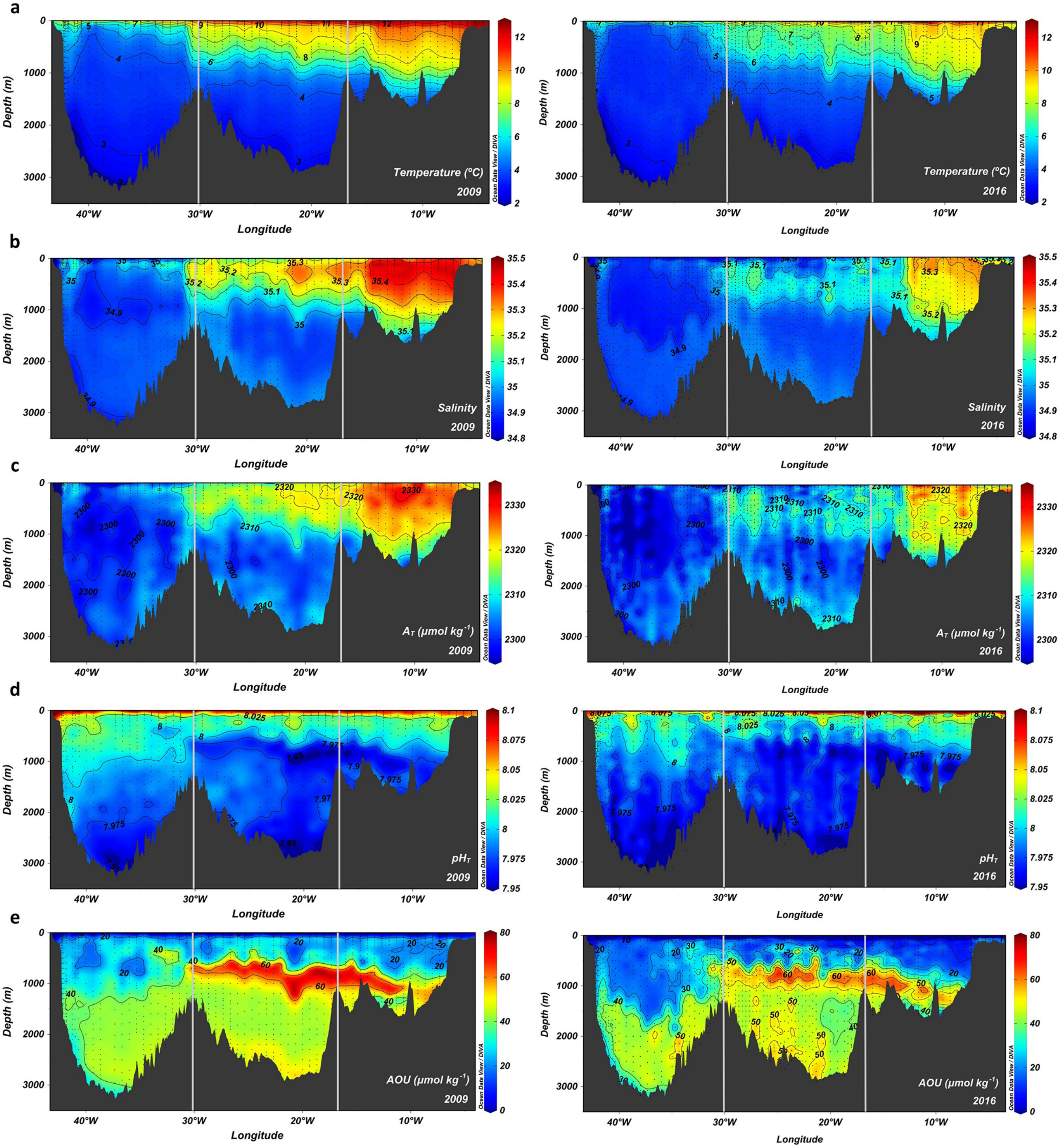

Figure 2. Water column distribution along the longitudinal transect of **(a)** temperature, **(b)** salinity, **(c)** A_T, **(d)** pH_T, and (e) AOU for the cruises of 2009 (left plots) and 2016 (right plots). The vertical white lines show the limits between basins. Figure produced with Ocean Data View (Schlitzer, Reiner, Ocean Data View, https://odv.awi.de, last access: 9 December 2024, 2021).

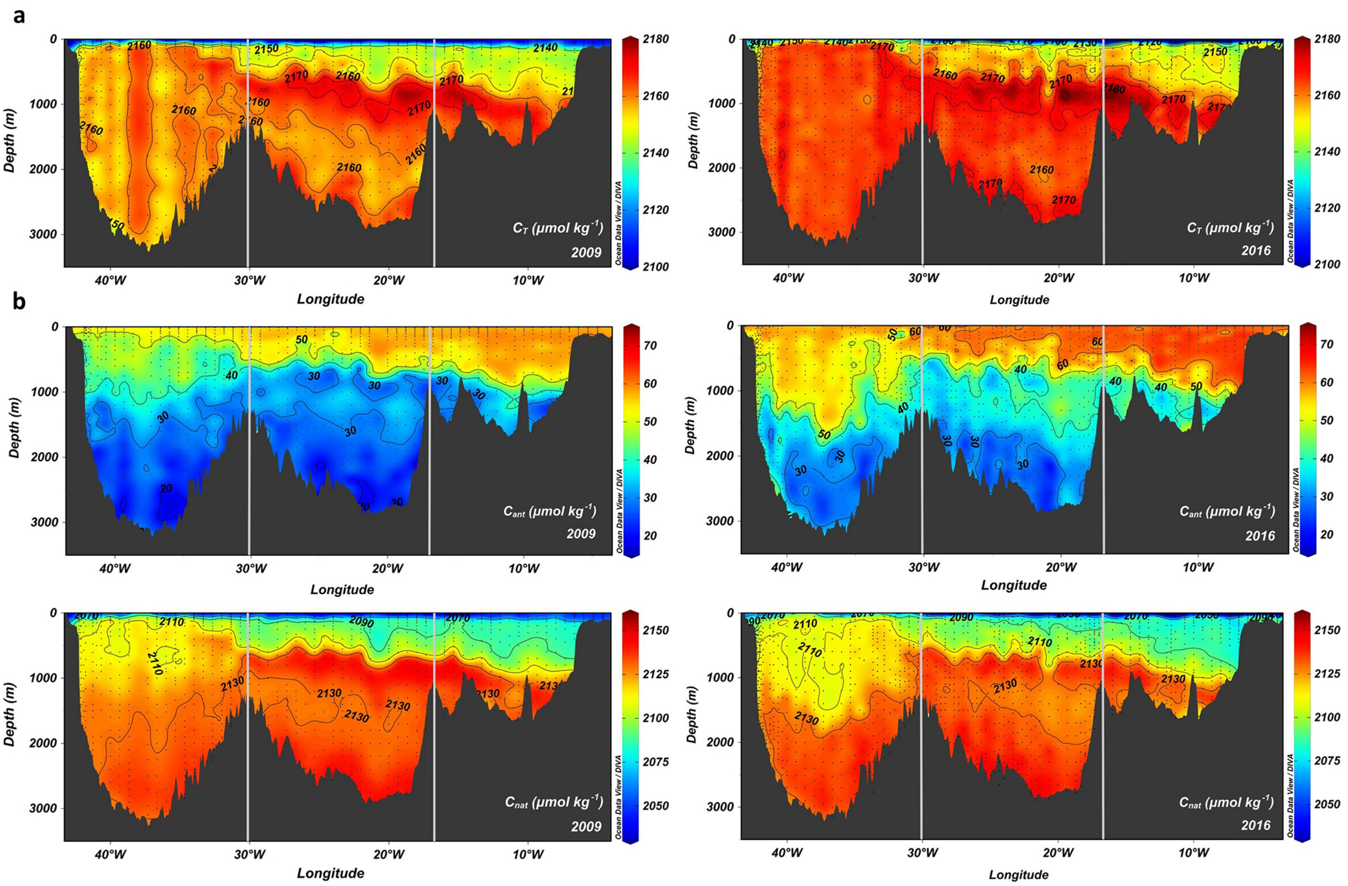

Figure 3. Water column distribution along the longitudinal transect of **(a)** C_T, **(b)** C_{ant}, and **(c)** C_{nat} for the cruises of 2009 (left plots) and 2016 (right plots). The vertical white lines show the limits between basins. Figure produced with Ocean Data View (Schlitzer, Reiner, Ocean Data View, https://odv.awi.de, last access: 9 December 2024, 2021).

tion, while low AOU values indicate the opposite. The slow renewal of waters with high AOU favours the accumulation of the product of remineralization (de la Paz et al., 2017). Thus, the areas with higher AOU (Fig. 2e) were found to have a high concentration of C_T and a low pH_T (Figs. 3a and 2d, respectively). The near-surface waters permanently in contact with the atmosphere exhibited the lowest AOU values ($< 20\,\mu mol\,kg^{-1}$). The Irminger Basin presents the most significant water column ventilation among the entire section, with maximum AOU ranging from 35 to $50\,\mu mol\,kg^{-1}$ at the LSW and ISOW and the remarkable intrusion of oxygenated DSOW ($> 260\,\mu mol\,kg^{-1}$ DO) over the continental slope with AOU ranging from 30 to $40\,\mu mol\,kg^{-1}$. The intermediate and deep layers of the Iceland and Rockall basins were less ventilated, with AOU values higher than 45–$50\,\mu mol\,kg^{-1}$. The thermocline layer placed between 500 and 1000 m depth along these two basins presented the highest maximum AOU throughout the period ($> 60\,\mu mol\,kg^{-1}$). The stagnation of these waters corresponds with the high C_T and low pH_T (Figs. 3a and 2d, respectively) encountered at intermediate depths and should be considered in their temporal evolution.

The temporal distribution and trends of the average physicochemical properties (Figs. 4, 5, 6, S4, S5, and S6) revealed remarkable heterogeneities in their interannual evolution within the period 2009–2019 among the different basins and water masses. The interannual trends are presented along with their respective standard error of estimate and correlation factors (r^2 and p-value) in Tables 2 and S4. The observed decrease in temperature and salinity, which was more pronounced in subsurface layers, and its implication on the MCS variations are discussed in Sect. 4.

4 Discussion

4.1 Reversal of the physical trends during 2009–2019

The present investigation revealed the cooling and freshening of the upper ocean in the NASPG within the period 2009–2019 (Fig. 4; Table 2), as recently reported since the reversal of climatic trend and surface physical properties occurring

Table 2. Interannual trends in temperature, salinity, C_T, C_{ant}, C_{nat}, pH_T, Ca, and Arag in each of the layers and basins. The ratios of change are based on linear regressions applied to the average values (as represented in Figs. 4–7) and are presented together with their standard error of estimate. The correlation coefficients (r^2) and p-values are also provided. Values in bold denote trends statistically significant at the 95 % level of confidence.

Basin	Layer	Temperature			Salinity			C_T			C_{ant}		
		Ratio (°C yr^{-1})	r^2	p-value	Ratio (psu yr^{-1})	r^2	p-value	Ratio (µmol kg^{-1} yr^{-1})	r^2	p-value	Ratio (µmol kg^{-1} yr^{-1})	r^2	p-value
Irminger	SPMW	−0.058 ± 0.024	0.60	0.02	−0.006 ± 0.003	0.59	0.03	0.62 ± 0.23	0.66	0.02	0.95 ± 0.17	0.89	< 0.01
	uLSW	−0.014 ± 0.011	0.30	0.16	−0.002 ± 0.001	0.59	0.03	1.02 ± 0.18	0.89	< 0.01	1.48 ± 0.29	0.87	< 0.01
	LSW	−0.010 ± 0.008	0.31	0.15	−0.002 ± 0.001	0.50	0.05	0.98 ± 0.26	0.78	< 0.01	1.53 ± 0.23	0.92	< 0.01
	ISOW	−0.002 ± 0.003	0.11	0.42	0.000 ± 0.000	0.00	0.99	0.90 ± 0.34	0.64	0.02	1.18 ± 0.29	0.81	< 0.01
	DSOW	−0.008 ± 0.008	0.22	0.25	0.001 ± 0.001	0.43	0.08	1.32 ± 0.23	0.90	< 0.01	1.77 ± 0.32	0.89	< 0.01
Iceland	SPMW	−0.074 ± 0.022	0.74	< 0.01	−0.013 ± 0.002	0.89	< 0.01	0.85 ± 0.64	0.32	0.15	1.02 ± 0.31	0.74	< 0.01
	uLSW	−0.012 ± 0.005	0.63	0.02	−0.002 ± 0.000	0.76	< 0.01	0.68 ± 0.22	0.71	< 0.01	1.42 ± 0.38	0.78	< 0.01
	LSW	0.005 ± 0.003	0.43	0.08	0.000 ± 0.000	0.28	0.18	0.88 ± 0.22	0.80	< 0.01	1.18 ± 0.35	0.75	< 0.01
	ISOW	−0.003 ± 0.006	0.05	0.61	−0.001 ± 0.000	0.47	0.05	0.98 ± 0.17	0.89	< 0.01	1.20 ± 0.32	0.79	< 0.01
Rockall	ENACW	−0.073 ± 0.061	0.27	0.19	−0.017 ± 0.004	0.80	< 0.01	0.05 ± 0.57	0.00	0.92	0. ± 0.11	0.94	< 0.01
	SPMW	−0.085 ± 0.019	0.84	< 0.01	−0.013 ± 0.003	0.85	< 0.01	0.86 ± 0.46	0.48	0.05	0.87 ± 0.18	0.86	< 0.01
	LSW	−0.020 ± 0.016	0.29	0.17	−0.002 ± 0.001	0.30	0.16	0.35 ± 0.29	0.27	0.19	1.38 ± 0.34	0.81	< 0.01

Basin	Layer	C_{nat}			pH_T			Ω_{Ca}			Ω_{Arag}		
		Ratio (µmol kg^{-1} yr^{-1})	r^2	p-value	Ratio (10^{-3} units yr^{-1})	r^2	p-value	Ratio (units yr^{-1})	r^2	p-value	Ratio (units yr^{-1})	r^2	p-value
Irminger	SPMW	−1.00 ± 0.42	0.60	0.02	−1.25 ± 0.93	0.32	0.14	−0.011 ± 0.006	0.50	0.05	−0.007 ± 0.003	0.53	0.04
	uLSW	−0.47 ± 0.38	0.28	0.18	−2.62 ± 0.69	0.79	< 0.01	−0.008 ± 0.005	0.40	0.09	−0.006 ± 0.003	0.44	0.08
	LSW	−0.54 ± 0.30	0.46	0.06	−3.17 ± 0.52	0.91	< 0.01	−0.014 ± 0.003	0.85	< 0.01	−0.009 ± 0.002	0.85	< 0.01
	ISOW	−0.27 ± 0.20	0.32	0.14	−2.97 ± 0.70	0.83	< 0.01	−0.010 ± 0.003	0.73	< 0.01	−0.007 ± 0.002	0.74	< 0.01
	DSOW	−0.32 ± 0.33	0.19	0.28	−2.41 ± 0.87	0.67	< 0.01	−0.004 ± 0.003	0.39	0.10	−0.003 ± 0.002	0.46	0.07
Iceland	SPMW	−0.19 ± 0.74	0.02	0.75	−2.32 ± 1.63	0.34	0.13	−0.016 ± 0.010	0.37	0.11	−0.010 ± 0.007	0.39	0.10
	uLSW	−0.74 ± 0.21	0.75	< 0.01	−2.31 ± 1.01	0.58	0.03	−0.009 ± 0.005	0.46	0.07	−0.006 ± 0.003	0.47	0.06
	LSW	−0.26 ± 0.26	0.20	0.27	−2.26 ± 1.06	0.54	0.04	−0.008 ± 0.005	0.41	0.09	−0.005 ± 0.003	0.41	0.09
	ISOW	−0.23 ± 0.21	0.23	0.23	−2.58 ± 0.99	0.64	< 0.01	−0.007 ± 0.004	0.42	0.08	−0.005 ± 0.003	0.43	0.08
Rockall	ENACW	−0.84 ± 0.50	0.43	0.08	−0.58 ± 2.31	0.02	0.77	−0.012 ± 0.013	0.18	0.30	−0.008 ± 0.008	0.19	0.28
	SPMW	−0.07 ± 0.59	0.00	0.88	−2.43 ± 1.90	0.30	0.16	−0.021 ± 0.013	0.38	0.10	−0.013 ± 0.008	0.39	0.10
	LSW	−1.05 ± 0.24	0.84	< 0.01	−1.36 ± 0.97	0.34	0.13	−0.008 ± 0.004	0.45	0.07	−0.005 ± 0.003	0.45	0.07

after 2005 (Holliday et al., 2020; Josey et al., 2018; Robson et al., 2016; Tesdal et al., 2018). The temperature decreased in the upper ocean (with more than 95 % level of confidence in SPMW, while not statistically significant in ENACW) by 0.05–0.08 °C yr^{-1} (Table 2), which is consistent with the ratio of heat loss per decade among the first 700 m depth equivalent to approximately −0.45 °C $decade^{-1}$ (−0.045 °C yr^{-1}) encountered over the period 2005-2014 (Robson et al., 2016). The interannual temperature trends in subsurface layers (Table 2) similarly draw the cooling observed in the Irminger basin between 2008 and 2017 (−0.05 and −0.11 °C yr^{-1} for summer and winter, respectively; Leseurre et al., 2020) and the winter average surface cooling along the entire NASPG between 2004 and 2017 (−0.08 ± 0.02 °C yr^{-1}; Fröb et al., 2019). The decrement in subsurface salinity (with more than 95 % level of confidence in both SPMW and ENACW) of 0.006–0.018 yr^{-1} (Table 2) agreed with the interannual rates provided by Tesdal et al. (2018) for the Irminger basin (−0.007 ± 0.002 yr^{-1}) and for the central eastern NASPG (−0.020 ± 0.003 yr^{-1}) over the period 2004–2015.

The fluctuations in physical properties were linked to a decrease in oceanic heat transport and storage within the NASPG, which has been attributed to changes in the AMOC over decadal to multidecadal timescales (Balmaseda et al., 2007; Desbruyères et al., 2013; Mercier et al., 2015; Smeed et al., 2018). However, the assessment of the temporal evolution of the AMOC in high latitudes remains uncertain, and there is no evidence of its impact on physical patterns across the NASPG on an interannual scale (Jackson et al., 2022). The changes in the atmospheric forcing also account for the variability in the upper-ocean physical properties and can have a cumulative effect over several years (Balmaseda et al., 2007; Böning et al., 2006; Eden and Willebrand, 2001; Marsh et al., 2005).

The distribution of the water mass properties, the processes of vertical and horizontal mixing, and the circulation patterns in the Irminger and Iceland basins were described by García-Ibáñez et al. (2016, 2018). The poleward path of the ENACW (Pollard et al., 1996) and its mixing with waters moving from the west across the NASPG (Ellett et al., 1986) accounted for the highest subsurface temperature and salinity signals observed in the Iceland basin and even more in the Rockall Trough. The SPMW and LSW in the Rockall Trough exhibited higher temperature and salinity signals in the order of ∼ 1 °C and ∼ 0.05–0.1, respectively, compared to the Irminger and Iceland basins (Fig. 4). The NASPG circulation patterns account for these differences by the eastward transport of these water masses, which subduct below the ENACW in the Rockall Trough and mix with warmer and more saline intermediate waters (i.e. Mediterranean Water) moving from the south (e.g. Ellett et al., 1986; Harvey, 1982; Holliday et al., 2000).

The low temperature and salinity signals in the less stratified Irminger basin (Fig. 2) experienced weaker interannual decreases in subsurface layers and higher rates of cooling

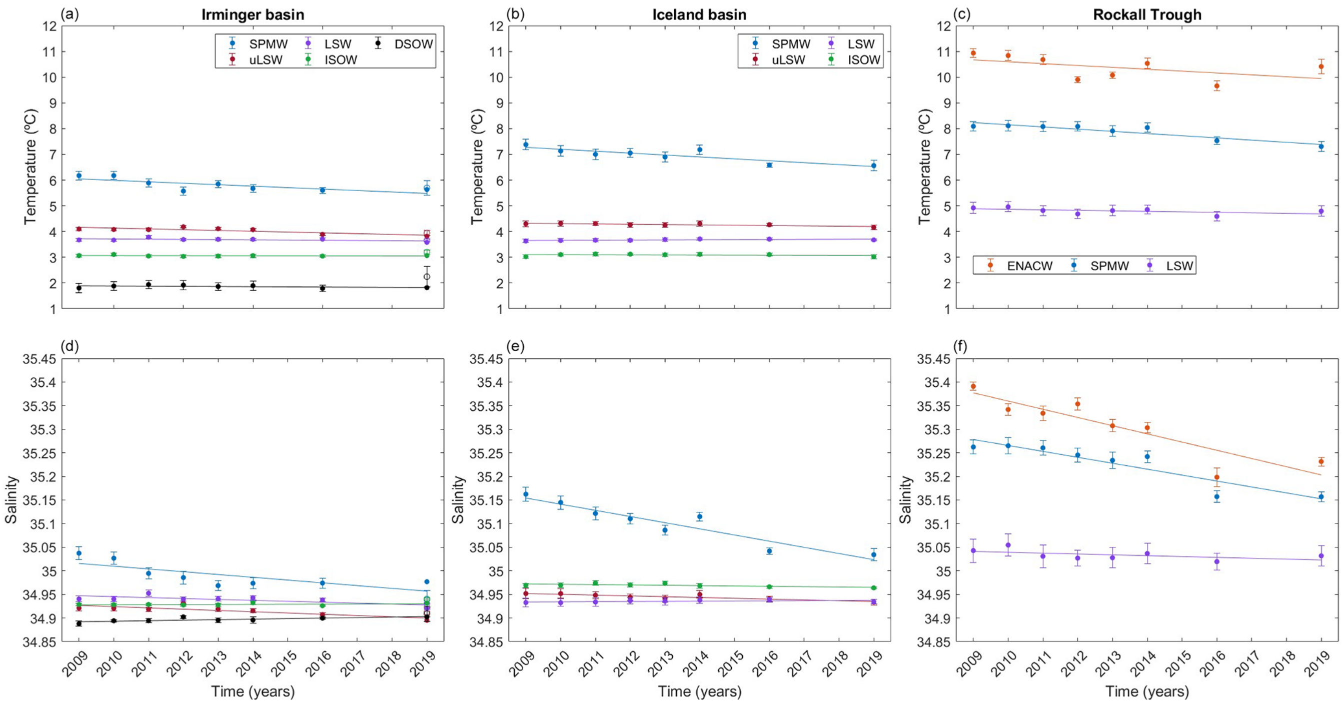

Figure 4. Temporal distribution (2009–2019) of the average temperature and salinity in each of the layers considered for the Irminger **(a, d)**, Iceland **(b, e)**, and Rockall basins **(c, f)**. The average values were calculated for each cruise and layer and are represented with coloured points together with their respective error bars at the time of each cruise (the method used for calculations is described in Sect. 3.2). In the Irminger plots, the empty points represent the average values for 2019 calculated with the measured data available in the easternmost part of the basin (sampled part during this cruise), while the coloured points for 2019 represent the average values corrected with A25-OVIDE-2018 data. The interannual trends are given by the linear regression of the average values, with the values of the slope, the standard error of estimate, and the r^2 presented in Table 2.

and freshening in intermediate and deep waters compared with the Iceland and Rockall basins (Fig. 4; Table 2). These longitudinal thermohaline heterogeneities were related to the enhancement of vertical mixing processes in areas of water mass formation along the western NASPG (Fröb et al., 2016; García-Ibáñez et al., 2015; Pickart et al., 2003; Piron et al., 2017) and to the water mass transformation along the NAC (Brambilla and Talley, 2008). The strongest decrement in subsurface temperature and salinity along the Iceland and Rockall basins (Fig. 4; Table 2) coincided with the significant event of heat loss and freshening observed by Holliday et al. (2020) in the eastern NASPG over the period 2012–2016, the so-called Great Salinity Anomaly. This pattern was not easily discernible in the Irminger basin due to the transport of freshwater through the Fram Strait and due to the redirection of the Labrador Current combined with changing wind stress curl (Holliday et al., 2020).

4.2 Evaluation of the interannual trends in C_T in response to changes in C_{ant} and C_{nat}

The changes in the physical patterns influenced the interannual variability in the MCS. The increase in C_T expected in the upper ocean due to the atmospheric CO_2 uptake was offset by the cooling and freshening (and dealkalinization) of the subsurface layers. The observed rates of increase in C_T (Table 2) did not show notable differences with respect to the interannual trends determined from previous decades in the Irminger and Iceland basins (0.62–0.82 and 0.38–0.64 µmol kg^{-1} yr^{-1}, respectively; García-Ibáñez et al., 2016) and at IRM-TS and IS-TS (0.49–0.71 and 0.39-0.94 µmol kg^{-1} yr^{-1}, respectively; Pérez et al., 2021). The interannual rates of increase in NC_T were higher than those of C_T in the subsurface layers, while the trends were similar among the intermediate and deep layers (Table 2). A detailed description of the interannual A_T trends is provided in Appendix B.

The entrance of C_{ant} through the air–sea interface and its accumulation dominated the observed increase in C_T (Fig. 5 and Table 2). The increase in ventilation over 2009–2019, shown by the negative AOU trends (Fig. S6 and Table S4), favoured the vertical mixing. The upper waters, due to be in contact with the atmosphere and have high biological production rates during the warm months, show high C_{ant} and low C_{nat} contents. The enhanced transport of upper waters toward the interior ocean explained the rapid growth in C_{ant} at intermediate and deep layers. The C_{ant} trends ranged between 0.85 and 1.77 µmol kg^{-1} yr^{-1} (statistically significant at the 99 % level). They were higher than those observed on a decadal to multidecadal scale since the late 20th century in the Irminger and Iceland basins (0.21–0.89 μmol kg^{-1} yr^{-1} during 1991–2015; García-Ibáñez et al., 2016; and 0.38–1.15 μmol kg^{-1} yr^{-1} during 1983–2013; Pérez et al., 2021), which show the enhancement in the C_{ant} accumulation on interannual scales during periods of high ventilation, as previously reported by Pérez et al. (2008). The C_{nat} shows an inverse relationship with C_{ant} at intermediate and deep layers ($r^2 > 0.5$; statistically significant at the 95 % level of confidence) and weakly decreased across the western deep-convection NASPG (Fig. 5 and Table 2). The growth in phytoplankton biomass (Ostle et al., 2022), together with the enhanced export toward the interior ocean under increasing ventilation, accounts for the observed decrease in C_{nat} in upper waters. The C_{nat} showed a weaker decrease at intermediate and deep layers due to the dominance of remineralization, which was not intense enough at this time of the year to neutralize the downward transport of low-C_{nat} water from the surface but partially compensated for its effect. The observed variations in C_{nat} between years, which were strongly linked with fluctuations in the biological processes, explained its non-significant trends at several layers. The changes in the circulation pattern of the NASGP, and thus in the horizontal advection related with the climatological forcing (Balmaseda et al., 2007; Desbruyères et al., 2013; Mercier et al., 2015; Thomas et al., 2008; Xu et al., 2013), could behave as a source of variability for both C_{ant} and C_{nat} and also implies differences between consecutive years.

The vertical distribution of C_{ant} and C_{nat} along the transect (Fig. 3b and c) reflects the higher stratification in the Iceland and Rockall basins compared to the well vertically mixed Irminger basin. It represents a source of variability in the interannual changes in C_{ant} among the different layers and basins (Fig. 4; Table 2). In the western NASPG, the surface heat loss and enhanced deep convection processes favour the solubility and subsequent uptake of atmospheric CO_2 and inject oxygenated and CO_2-rich waters into deeper layers (Messias et al., 2008). It likely accounts for intermediate and deep layers in the Irminger basin exhibiting the highest C_{ant} accumulation rates in the NASPG (Fig. 5; Table 2). The highest ventilation of the interior ocean in the Irminger basin was demonstrated by its minimum AOU values (Figs. 2 and S6). It induced a rapid surface-to-bottom transport of C_{ant} shown by its highest rates of increase in intermediate and deep waters throughout the region (Fig. 5; Table 2). The high C_{ant} values and their rapid increment at DSOW were explained by the improved oxygenation of this layer at shallower depths (interannual AOU trends given in Table S4) and its subduction through the continental slope below ISOW.

In the eastern NASPG, the stratification weakened due to the path of the NAC warming the upper water column eastward and accounted for slowing down the increase in C_{ant} in the Iceland basin. An exception is the Rockall basin, in which the relatively warm and salty ENACW (Figs. 2 and 4) showed the maximum C_{ant} (58–68 μmol kg^{-1}) and minimum C_{T} (2120–2131 μmol kg^{-1}) and C_{nat} (2058–2070 μmol kg^{-1}) throughout the region (Figs. 3 and 5). The enhanced oxygenation of the ENACW (AOU < 20 μmol kg^{-1} and reaching the oxygen saturation after 2014) was related, with its high rates of renovation due to its path from the south (Pollard et al., 1996) and its mixing with waters moving eastward (Ellett et al., 1986). This favoured the transport of subsurface waters with relatively high C_{ant} content from lower latitudes into the Rockall Trough and introduced wide differences with respect to adjacent deeper layers moving from the western NASPG, which strengthened the stratification. As the NAC transports nutrient-rich waters northward and eastward into subsurface layers in the Rockall Trough, biological production tends to increase, and it actively reduced the CO_2 excess from the ENACW (McGrath et al., 2012b), as proved by the observed low C_{T} and C_{nat}. The ENACW presented relatively low C_{nat} and C_{T} (Fig. 5) and high A_{T} and NA_{T} in 2014. These variations indicated that the increase in carbonate and bicarbonate concentrations raising A_{T} and NA_{T} was compensated for by the depletion in dissolved CO_2. The relatively high temperature and NA_{T} in 2014 likely indicated an improved spreading of subsurface waters from subtropical latitudes into the Rockall Trough. The enhanced biological production in these waters, together with the reduction in solubility due to warming which favours the CO_2 evasion to the atmosphere, accounts for the decreasing C_{nat} and thus C_{T}.

The strong interannual increase in the ENACW ventilation during this decade increased the C_{ant} and decreased the C_{nat} (Rodgers et al., 2009), keeping the C_{T} approximately constant (Table 2). The poorly ventilated thermocline (AOU > 60 μmol kg^{-1}), placed between 500–1000 m in the eastern NASPG, induced a C_{nat}-driven increase in C_{T} among the SPMW and uLSW. However, its intrusion does not present relevant variations with time and thus does not introduce differences in the interannual trends in the biogeochemical properties.

4.3 Acidification trends

The interannual pH_{T} trends (Fig. 6, Table 2) exhibited the acidification of the whole water column in NASPG during the period 2009–2019. Despite the acidification rates observed in most subsurface waters among the three basins not being significant at the 90 % confidence level (Table 2), they were consistent in the interval of 0.001 units yr^{-1} with the rates observed during longer periods at time series stations located across the North Atlantic: at subtropical latitudes (0.0018 ± 0.0002 units yr^{-1} during 1995–2014 and 0.0020 ± 0.0001 units yr^{-1} during 1995-2023 at ESTOC; González-Dávila and Santana-Casiano, 2023; and 0.0017 ± 0.0001 units yr^{-1} during 1983–2014 at BATS; Bates et al., 2014) and subpolar latitudes (-0.0017 ± 0.0002 units yr^{-1} at IRM-TS during 1983–2013

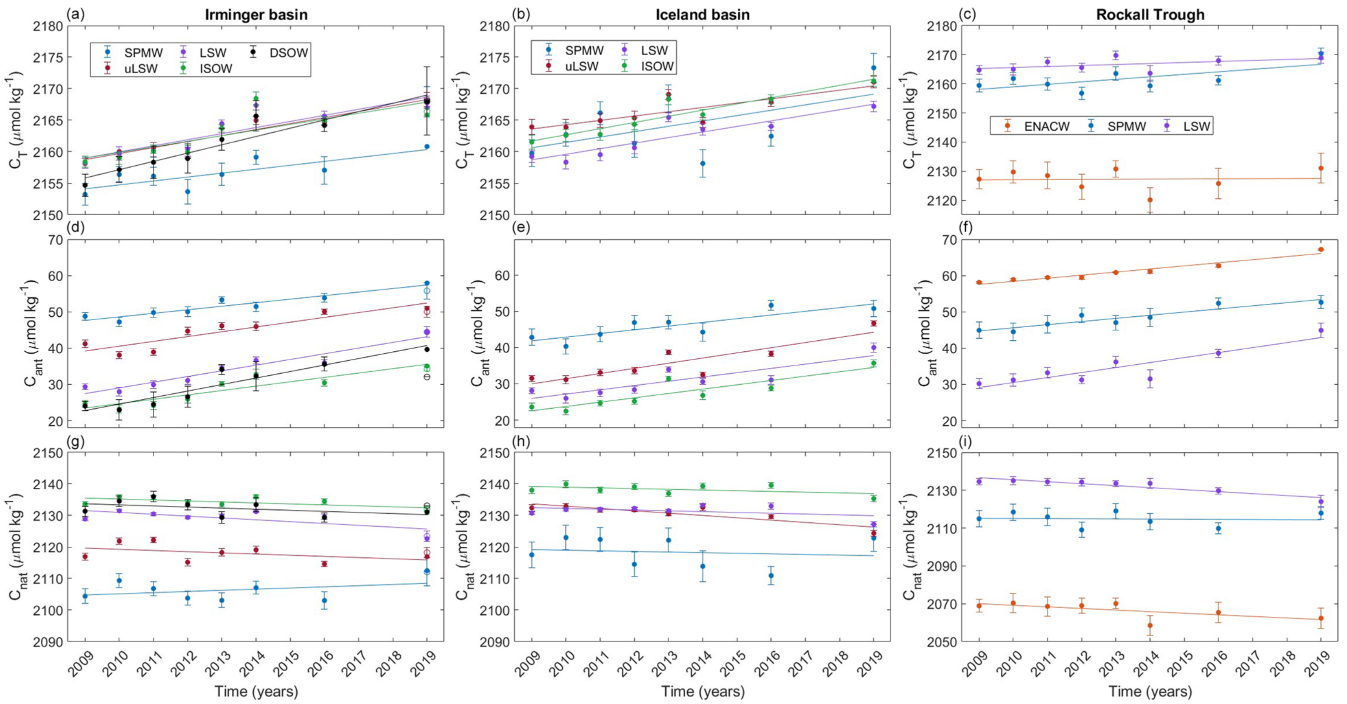

Figure 5. Temporal distribution (2009–2019) of the average C_T, C_{ant}, and C_{nat} in each of the layers considered for the Irminger **(a, d, g)**, Iceland **(b, e, h)**, and Rockall basins **(c, f, i)**. The average values were calculated for each cruise and layer and are represented with coloured points together with their respective error bars at the time of each cruise (the method used for calculations is described in Sect. 3.2). In the Irminger plots, the empty points represent the average values for 2019 calculated with the measured data available in the easternmost part of the basin (sampled part during this cruise), while the coloured points for 2019 represent the average values corrected with A25-OVIDE-2018 data. The interannual trends are given by the linear regression of the average values, with the values of the slope, the standard error of estimate, and the r^2 presented in Table 2.

and -0.0026 ± 0.0002 units yr^{-1} at IS-TS during 1985–2013, summarized by Pérez et al., 2021). In addition, the changes in the surface pH_T trends were reported by Leseurre et al. (2020) in the western NASPG within a wide latitudinal area (54–64° N) during the period 2008–2017 in comparison with the periods 1993–1997 and 2001–2007. However, the highly significant cooling observed in SPMW, the year-to-year variations in ventilation (shown by the annual average AOU and its trends in Fig. S6), and thus the variations in C_{nat} and C_{ant} (Fig. 5) introduced relevant changes in pH_T on an interannual scale and explained the low-significance trends. The extremely negative NAO index of 2009–2010 (Jung et al., 2011) weakened the wind forcing, which implies variability in the circulation patterns and physical properties of the surface waters, consequently reducing deep convection. This was observed in the slowdown in ventilation from 2009–2010 (Fig. S6) in the Irminger and Iceland basins which caused a relative increase in C_{nat} and decrease in C_{ant} (Fig. 5).

The highest acidification rates were found through intermediate and deep waters in the Irminger and Iceland basins, coinciding with the highest rates of increase in C_{ant} (Table 2; trends statistically significant at more than 95 % level of confidence). The exception is the DSOW, which presented an interannual decrease in pH_T in phase with that of the uLSW. This singularity was previously observed by García-Ibáñez et al. (2016), who noticed the similar trends between the DSOW and LSW attributed to the recent formation and sink through the continental slope of the DSOW. The acidification rates found among the uLSW, LSW, and ISOW (0.0026–0.0032 units yr^{-1}) experienced, on an interannual scale, an acceleration in comparison with previous reports based on long-term records (e.g. 0.0009–0.0017 units yr^{-1} estimated for 1981–2008 by Vázquez-Rodríguez et al. (2012b); 0.0013–0.0016 units yr^{-1} estimated for 1991–2015 by García-Ibáñez et al., 2016; 0.0015–0.0019 units yr^{-1} estimated for 1983–2013 at the IRM-TS by Pérez et al., 2021; and 0.0019 ± 0.0001 units yr^{-1} estimated for 1993–2017 by Leseurre et al., 2020). Contrasting the rates of change in pH_T during the decade of study with those encountered by these multidecadal evaluations (and considering the total number of years comprising each of the studies and the changes in the ion hydrogen concentration $[H^+_T]$), we estimate an acceleration in the rates of acidification of 0.4 %–5.4 % in the Irminger basin and 1.0 %–9.0 % in the Iceland basin during the 2010s since the late 20th century. This acceleration was mainly attributed to increased deep-water ventilation (shown in the rapid decrease in AOU in Fig. S6) favouring the progressive increase in the accumu-

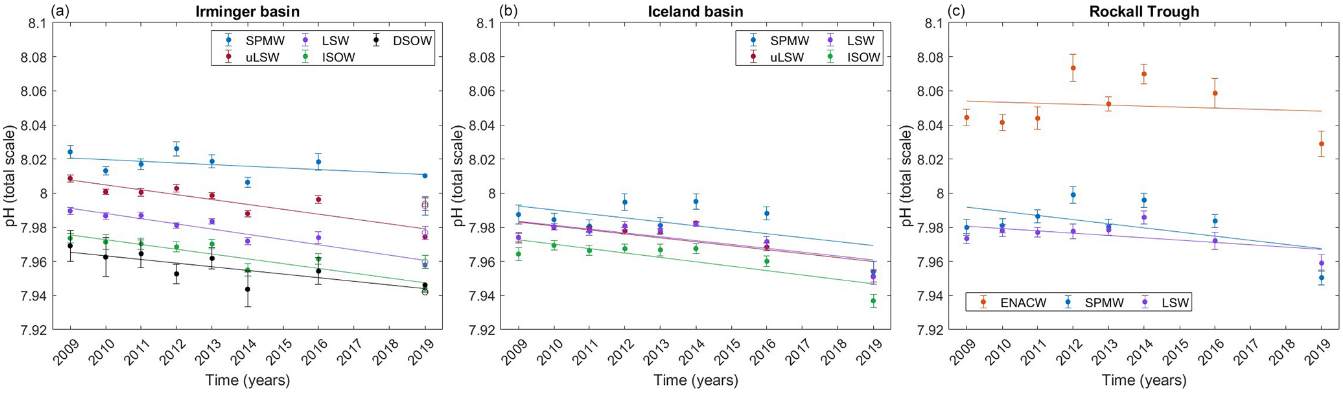

Figure 6. Temporal distribution (2009–2019) of the average pH_T (in situ temperature) in each of the layers considered for the Irminger **(a)**, Iceland **(b)**, and Rockall basins **(c)**. The average values were calculated for each cruise and layer and are represented with coloured points together with their respective error bars at the time of each cruise (the method used for calculations is described in Sect. 3.2). In the Irminger plots, the empty points represent the average values for 2019 calculated with the measured data available in the easternmost part of the basin (sampled part during this cruise), while the coloured points for 2019 represent the average values corrected with A25-OVIDE-2018 data. The interannual trends are given by the linear regression of the average values, with the values of the slope, the standard error of estimate, and the r^2 presented in Table 2.

lation of C_{ant} and C_{nat} toward intermediate deep layers, in which cooling was not significant in the Irminger basin and not intense enough in both basins to compensate the acidification.

Despite the similarities encountered in the pH_T trends among both basins, the average values presented differences which may be closely linked with the transport and transformation of the water masses along the NASPG and mainly modulated by the Reykjanes Ridge (García-Ibáñez et al., 2015, 2016, 2018). The transformation of the SPMW formed in the Iceland basin (McCartney and Talley, 1982; Brambilla and Talley, 2008; Tsuchiya et al., 1992; van Aken and Becker, 1996) and flowing with the NAC across the Reykjanes Ridge (Brambilla and Talley, 2008) accounted for the lower pH_T values in the Irminger basin. The differences in pH_T found at intermediate and deep layers were related to the divergence of the LSW path into two cores when it reaches the Reykjanes Ridge (Álvarez et al., 2004; Pickart et al., 2003) and the ISOW path flowing southward along the western Iceland basin and recirculating northward into the eastern Irminger basin (Dickson and Brown, 1994; Saunders, 2001). These differences in the spreading of water masses enhanced the ventilation in the Irminger basin favouring the fall in pH_T compared with the Iceland basin. The rise in the ISOW following the Reykjanes Ridge slope through its eastern flank favoured a strong vertical mixing over and around the ridge (Ferron et al., 2014) and a reduction in the LSW core in the Iceland basin (García-Ibáñez et al., 2015), contributing to the resemblance of pH_T values and trends among the uLSW and LSW in this basin.

The upper waters of the Rockall Trough presented the maximum pH_T throughout the transect (8.02–8.08 units). The observed strong pH_T fluctuations between years related to interannual changes in the NAC do not allow us to discern trends with an interval of confidence equal to or greater than 90 %. The interannual decrease in pH_T in the ENACW (~ 0.001 units yr^{-1}) was half that observed along southernmost transects in the Rockall Trough between 1991 and 2010 (~ 0.002 units yr^{-1}; McGrath et al., 2012a). The temporal distribution of the average pH_T (Fig. 6), highly influenced by the high ventilation (seen in minimum AOU values that are highly variable between years and which tend to decrease with 99 % statistical confidence; Fig. S6 and Table S4), allows us to discern two periods: the approximately constant ventilation rates keep a steady state in terms of pH_T during 2009–2011, while the progressive renewal and oxygenation of subsurface waters after 2012 (and peaking in this year) increase the pH_T. The renewal of waters in the shallow Rockall Trough, in contrast with the westernmost NASPG, was primarily driven by lateral rather than vertical advection. The modifications of the ENACW through air–sea exchange and mixing with adjacent waters modulated its properties at different timescales (Holliday et al., 2000) and caused the observed variations in the MCS. The variations in pH_T between consecutive years after 2012 may be attributed to the fluctuations in the spreading into the Rockall Trough of several water masses occupying different depths coming from the south and east (Ellett et al., 1986; Pollard et al., 1996). Holliday et al. (2020) reported the reduction in the spreading of saline subsurface waters from subtropical latitudes and the diversion of Arctic freshwater from the western boundary into the eastern NASPG during 2012–2016. The subsequent freshening of the ENACW compensated for the increase in A_T expected without the effect of salinity (seen in the decreasing A_T against the increasing NA_T; Fig. S4 and Table S4) and weakened the increase in C_T expected due to poleward advection (see in the slowdown in the rise of C_T in comparison to that of NC_T; Figs. 5 and S5 and Tables 2 and S4). The C_T remains approximately constant (Fig. 5 and Table 2) due to the increase in C_{ant} ($0.85 \pm 0.11\,\mu mol\,kg^{-1}\,yr^{-1}$; p-value < 0.01) being neutralized by the decrease in C_{nat} ($-0.84 \pm 0.50\,\mu mol\,kg^{-1}\,yr^{-1}$; p-value < 0.1). These findings suggest that the atmospheric CO_2 invasion was offset by the growing phytoplankton biomass favouring its biological uptake (Ostle et al., 2022) and by the weakening transport of remineralized and saline water from the south (Holliday et al., 2020), thus compensating for the acidification of the ENACW.

The SPMW among the Iceland and Rockall basins showed similar pH_T trends (Table 2) due to the emplacement of the poorly oxygenated thermocline at these depths (García-Ibáñez et al., 2016). The approximately constant AOU at SPMW in the eastern NASPG (Fig. S6) proved its steady ventilation, which can introduce differences in the acidification rates among the layers comprising the Rockall Trough. The influence of the cooling and freshening of deeper areas due to the spreading and horizontal mixing was notable in the LSW, which presented slightly higher pH_T values in the Rockall Trough with respect to the adjacent Iceland basin.

4.4 Interannual changes in Ω_{Ca} and Ω_{Arag}

The analysis of the changes in Ω_{Ca} and Ω_{Arag} hold significance in elucidating the potential effects of OA over the $CaCO_3$ species calcite and aragonite, thereby offering insights into their potential implications for marine calcifying organisms and ecosystems. The vertical distribution of Ω_{Ca} and Ω_{Arag} is presented in Fig. S3. The upper and intermediate layers up to 2100–2400 m depth of the Irminger and Iceland basins and the whole Rockall basin were supersaturated for aragonite ($\Omega_{Arag} > 1$), while the DSOW was undersaturated ($\Omega_{Arag} < 1$). The ISOW, with Ω_{Arag} ranging between 1.0 and 1.1 at the beginning of the decade, crossed to undersaturated conditions at the end of the decade due to the progressive rise of the aragonite saturation horizon (depth at which $\Omega_{Arag} = 1$). The whole water column throughout the section was supersaturated for calcite ($\Omega_{Ca} > 1$) due to its lower solubility (Mucci, 1983). The Ω_{Ca} and Ω_{Arag} in the SPMW (2.2–2.7 and 1.4–1.7 units, respectively) were lower than those encountered equatorward in the subsurface Atlantic (> 4.0 and > 2.5 units, respectively; González-Dávila et al., 2010; González-Dávila and Santana-Casiano, 2023). The poleward pathway of low-latitude upper waters through the Rockall Trough explained the higher Ω_{Ca} and Ω_{Arag} found in the ENACW (3.0–3.6 and 1.8–2.3 units, respectively). The reduction in Ω_{Ca} and Ω_{Arag} towards higher latitudes in the upper and intermediate layers smooths the vertical gradients in the NASPG compared to the subtropical latitudes (González-Dávila et al., 2010; González-Dávila and Santana-Casiano, 2023).

The correlation of Ω with pH_T ($r^2 = 0.90$) with a level of significance higher than 99 % explains that the individual components driving OA accompanied the decline in Ω. The interannual trends in Ω_{Ca} and Ω_{Arag} (Fig. 7, Table 2) exhibited the decrement through the whole water column along the NASPG with a level of statistical confidence generally higher than 90 %. The rates of decline for Ω_{Ca} and Ω_{Arag} in the SPMW (0.011–0.021 and 0.007–0.013 units yr^{-1}, respectively) were consistent with the trends observed up to 100 m depth at ESTOC between 1995 and 2023 (0.019 ± 0.001 and 0.012 ± 0.001 units yr^{-1}, respectively; González-Dávila and Santana-Casiano, 2023) and in surface waters at the IS-TS between 1985 and 2008 (0.0117 ± 0.0011 and 0.0072 ± 0.0007 units yr^{-1}, respectively; Olafsson et al., 2009). The Ω_{Arag} trend estimated for SPMW in the Irminger basin (-0.007 ± 0.003 units yr^{-1}) is consistent with that reported for surface waters by Bates et al. (2014) over 1983–2014 (-0.008 ± 0.004 units yr^{-1}) and falls within the range of those estimated during summer by Leseurre et al. (2020) over 2008–2017 (-0.005 ± 0.001 units yr^{-1}). Chau et al. (2014) recently deduced from reconstructed products a slower decrease (-0.004 ± 0.001 units yr^{-1}), highlighting the large uncertainty in the estimations of interannual trends for pH and Ω_{Arag} across the NASPG due to the low data-sampling frequency at their monitoring sites. The decline in Ω_{Arag} in the SPMW accelerated by ~ 26 % and ~ 51 % in the Irminger and Iceland basins, respectively, in comparison with the trends given for the period 1991–2018 (0.0052 ± 0.0006 and 0.0049 ± 0.0015 units yr^{-1}, respectively; García-Ibáñez et al., 2021). The observed decrease in Ω_{Arag} in the SPMW was ~ 23 % faster in the Rockall Trough than in the adjacent Iceland basin. The interannual decline in Ω_{Ca} and Ω_{Arag} in the ENACW (0.012 and 0.008 units yr^{-1}, respectively) agreed with these previous observations but were not statistically significant, likely due to the high variability modifying the changes in pH_T in this layer (see Sect. 4.2). Despite the acceleration of the acidification rates toward intermediate and deep layers, the declining rates weakened for Ω_{Ca} and even more for Ω_{Arag} (Table 2). Moreover, the vertical profiles were approximately constant throughout the section in contrast with the heterogeneous vertical distribution of pH_T between basins. This behaviour was previously observed in the Irminger and Iceland basins by García-Ibáñez et al. (2021) and explained by pressure- and temperature-induced changes in the speciation of the CO_2–carbonate chemistry species (Jiang et al., 2015) and in the solubility of calcite and aragonite (Mucci, 1983). Their combined action counterbalanced the alterations resulting from acidification, particularly in colder deep waters, where the solubility of calcite and aragonite was reduced (García-Ibáñez et al., 2021). However, the decrease in Ω_{Ca} and Ω_{Arag} along the uLSW, LSW, and ISOW accelerated by 40 %–75 % in relation to the trends reported by García-Ibáñez et al. (2021) for the Irminger and Iceland basins. The LSW and ISOW presented faster-declining rates for Ω_{Ca} and Ω_{Arag} in the Irminger basin (Table 2), which may be caused by the enhanced ventilation of the interior ocean which accelerated the acidification (see Sect. 4.2). The westward rise in the depth of these layers along the Greenland continental slope, accompanied by a subsequent elevation in the horizons of solubility, resulted in reduced buffering capacity against acidification effects in the Irminger basin when compared to the Iceland basin. In contrast, the rise in the depth of LSW in the Rockall Trough favours the increment of ~ 0.2 units in Ω_{Ca} and Arag with respect to the Iceland basin but had no influence on the interannual trends, which coincided. The Ω_{Ca} and Ω_{Arag} in the DSOW, despite showing a trend accelerated by $\sim 30\,\%$ compared to that observed by García-Ibáñez et al. (2021), presented the weakest interannual decreases throughout the section (0.004 ± 0.003 and 0.002 ± 0.001 units yr^{-1}, respectively) due to the high pressure and low temperatures compensating for the rapid acidification (Fig. 6, Table 2).

The decrease in Ω could have severe consequences on organisms reliant on aragonite, which is less resistant to dissolution than calcite (Mucci, 1983; Broecker and Peng, 1983) and is thus expected to experience relatively higher susceptibility to the effects of OA over shorter timescales (Raven et al., 2005). The progressive reduction in Ω_{Arag} has driven a long-term decrease in the depth of the aragonite saturation horizon ($\Omega_{Arag} = 1$) by 80–400 m since the preindustrial era (Álvarez et al., 2003; Feely et al., 2004; Pérez et al., 2013, 2018; Tanhua et al., 2007; Wallace, 2001) and is projected to shoal by more than 2000 m by the end of the century under the IS92a scenario (Orr et al., 2005). The vertical section of Ω_{Arag} in Fig. S3 shows the shallower aragonite saturation horizon during 2009 and 2016 compared to preindustrial times. Likewise, Orr et al. (2005) suggested that high-latitude surface waters could become undersaturated if the atmospheric CO_2 concentration doubles the preindustrial concentration within the next 50 years. This would reduce the calcification rates in some shallow calcifying organisms by more than 50 % (Feely et al., 2004).

The planktonic aragonite-producing pteropods (e.g. *Limacina helicina* and *Clio pyramidata*), which have high population densities in subpolar regions up 300 m depth (Bathmann et al., 1991; Urban-Rich et al., 2001) and play a key role in the export flux of both carbonate and organic carbon (Accornero et al., 2003; Collier et al., 2000), are expected to be highly vulnerable to OA if the aragonite saturation horizon continues to shoal (Orr et al., 2005). The undersaturation toward the intermediate and upper layers negatively influences the aragonite-based CWCs (e.g. *Lophelia pertusa* and *Madrepora oculata*), which show their highest diversity and population along the NASPG between 200 and 1000 m depth in the global ocean (Roberts et al., 2009). In fact, several studies reported that CWC ecosystems are anticipated to be among the first deep-sea ecosystems to experience acidification threats (Gehlen et al 2014; Guinotte et al., 2006; Maier et al., 2009; Raven et al., 2005; Roberts et al., 2009; Turley et al., 2007), particularly in the North Atlantic (Pérez et al., 2018). The findings presented here contribute to a deeper understanding of the biological impacts of OA along the NASPG.

4.5 Processes controlling OA and Ω trends

Due to the variety of processes involved in OA, a decomposition of the pH_T and trends into the individual components that govern their spatiotemporal variability took place (see Sect. 2.2.6). The interannual variations in pH_T ($\frac{dpH_T}{dt}$) and Ω ($\frac{d\Omega}{dt}$) explained by fluctuations in temperature ($\frac{\partial pH_T}{\partial T}\frac{\partial T}{dt}$ and $\frac{\partial \Omega}{\partial T}\frac{\partial T}{dt}$), salinity ($\frac{\partial pH_T}{\partial S}\frac{\partial S}{dt}$ and $\frac{\partial \Omega}{\partial S}\frac{\partial S}{dt}$), A_T ($\frac{\partial pH_T}{\partial A_T}\frac{\partial A_T}{dt}$ and $\frac{\partial \Omega}{\partial A_T}\frac{\partial A_T}{dt}$), and C_T ($\frac{\partial pH_T}{\partial C_T}\frac{\partial C_T}{dt}$ and $\frac{\partial \Omega}{\partial C_T}\frac{\partial C_T}{dt}$) were calculated for each layer and basin (Eq. 2) and are summarized in Tables 3 and 4. The positive contributions of each of the drivers indicate increments, while negative contributions indicate the opposite. The cumulative changes resulting from the distinct drivers (referred to with the subscript "calculated" in Tables 3 and 4) were consistent with the observed pH_T trends (referred to with the subscript "obs" in Tables 3 and 4), thereby instilling confidence in the methodology. An exception was found at the DSOW, in which the strong NA_T decrease had a crucial influence on the declining Ω.

The minimal differences between observed and calculated rates of change have added coherence to the non-significant trends identified for pH_T and Ω trends and/or their drivers in some basins and layers (Tables 2, 3, and S4). In the entire section at SPMW, the $\frac{dpH_T}{dt}$ (calculated), explained by the cumulative impact of its drivers (all of them statistically significant at the 95 % level of confidence), aligns within a range of < 0.0002 units yr^{-1} with $\frac{dpH_T}{dt}$ (obs) (which was not significant). In the Irminger and Iceland basins at intermediate and deep layers, the $\frac{dpH_T}{dt}$ (obs) (statistically significant at least at the 95 % level of confidence) was consistent within the range of < 0.001 units yr^{-1} with $\frac{dpH_T}{dt}$ (calculated) (T, S, and NA_T show non-significant trends at some of the intermediate and deep layers). The interannual variations were non-significant for pH_T for its drivers in the Rockall Trough at LSW and ENACW. The high temporal dispersion of average data in these layers was mainly related to the rise in depth of LSW along the eastern continental slope and its mixing with shallower waters coming from subtropical latitudes (Ellett et al., 1986; Harvey, 1982; Holliday et al., 2000). The substantial variability in the Rockall Trough made it difficult to discern OA patterns and its drivers on an interannual scale. Therefore, long-term monitoring and the development of multidecadal-scale studies are required in this area to derive significant conclusions.

The cooling and freshening modified the physically driven pH_T changes compared with those encountered by García-Ibáñez et al. (2016) during previous decades in the western NASPG. The cooling contributed to an increase in the pH_T and compensated for the observed acidification rate.

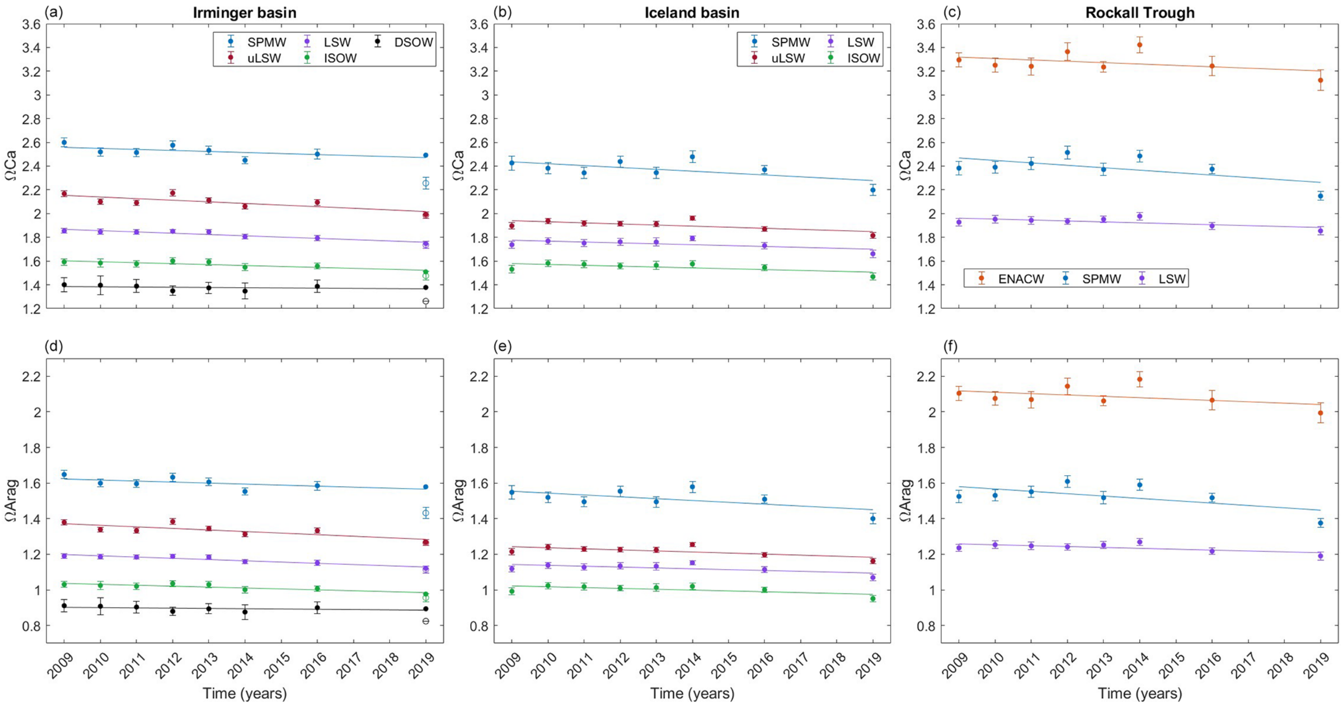

Figure 7. Temporal distribution (2009–2019) of the average Ca and Arag in each of the layers considered for the Irminger **(a, d)**, Iceland **(b, e)**, and Rockall basins **(c, f)**. The average values were calculated for each cruise and layer and are represented with coloured points together with their respective error bars at the time of each cruise (the method used for calculations is described in Sect. 3.2). In the Irminger plots, the empty points represent the average values for 2019 calculated with the measured data available in the easternmost part of the basin (sampled part during this cruise), while the coloured points for 2019 represent the average values corrected with A25-OVIDE-2018 data. The interannual trends are given by the linear regression of the average values, with the values of the slope, the standard error of estimate, and the r^2 presented in Table 2.

The increase in pH_T due to temperature fluctuations was at its maximum at SPMW (~ 0.001 units yr^{-1}) and negligible in deeper layers (< 0.0003 units yr^{-1} at uLSW and below). The increase in pH_T due to salinity fluctuations was minimal (< 0.0001 units yr^{-1}) through the whole water column in the three basins, reflecting that the observed freshening caused insignificant changes in pH_T. The temperature and salinity contributed by 19.1 %–26.5 % and 1.2 %–3.3 %, respectively, to the total pH_T change in the upper layers, while presented an influence 3 times lower toward the interior ocean (1.3 %–7.6 % and < 0.6 %, respectively). The enhanced convective processes in the Irminger basin (e.g. Fröb et al., 2016; García-Ibáñez et al., 2015; Gladyshev et al., 2016a, b; Piron et al., 2017), together with the rapid transport of LSW from the Labrador Sea to the Irminger basin (Yashayaev et al., 2007), introduced differences to the thermally driven pH_T in the Iceland basin, as previously reported by García-Ibáñez et al. (2016). The advection of LSW through the Greenland continental slope also affected the DSOW (Read, 2000; Yashayaev and Dickson, 2008), which shows thermally driven pH_T changes consistent with those encountered through the LSW in the Irminger basin.

Despite the negligible direct contribution of the salinity fluctuations over the pH_T changes, the freshwater fluxes influence the distribution of A_T and C_T, indirectly affecting pH_T trends. After removing salinity effects, NA_T shows positive trends in subsurface layers and negative trends toward the interior ocean (Fig. S4 and Table S4; detailed in Appendix B). The changes in NA_T described the 7.8 %–10.1 % of the total pH_T change at SPMW. The NA_T-driven pH_T changes weakened with depth (Table 3) due to the insignificantly interannual changes in NA_T through LSW and ISOW (Table S4). The weak contribution of NA_T in these layers (1.3 %–5.1 %) could be related to the difficulty in reversing the large alkalinization until the 2000s, resulting from the slowdown in the formation of LSW since the mid-1990s (Lazier et al., 2002; Yashayaev, 2007), which was transmitted towards deeper overflow waters (Sarafanov et al., 2010). The substantial interannual changes and the abrupt change between periods of increase and decrease in the seawater properties at DSOW (Yashayaev et al., 2003; Stramma et al., 2004) linked with changes in the LSW formation (Dickson et al., 2002) explain the rapid decrease in NA_T (Table S4), which explains the 14.6 % decline in the pH_T.

Table 3. Temporal changes in pH_T (in 10^{-3} units yr^{-1}) explained by fluctuations in temperature ($\frac{\partial pH_T}{\partial T}\frac{\partial T}{dt}$), salinity ($\frac{\partial pH_T}{\partial S}\frac{\partial S}{dt}$), A_T($\frac{\partial pH_T}{\partial A_T}\frac{\partial NA_T}{dt}$), and C_T($\frac{\partial pH_T}{\partial C_T}\frac{\partial NC_T}{dt}$) in each of the layers considered for the Irminger, Iceland, and Rockall basins during the period 2009–2019. The sum of the changes explained by the individual drivers represents the calculated interannual pH_T change ($\frac{dpH_T}{dt}$calculated), as detailed in Sect. 2.2.5. The observed interannual pH_T trends ($\frac{dpH_T}{dt}$observed), shown in Fig. 7 and provided in Table 2, are also added to the table for comparison.

Basin	Layer	$\frac{\partial pH_T}{\partial T}\frac{\partial T}{dt}$	$\frac{\partial pH_T}{\partial S}\frac{\partial S}{dt}$	$\frac{\partial pH_T}{\partial A_T}\frac{\partial NA_T}{dt}$	$\frac{\partial pH_T}{\partial C_T}\frac{\partial NC_T}{dt}$	$\frac{dpH_T}{dt}$ (obs)	$\frac{dpH_T}{dt}$ (calculated)
Irminger	SPMW	0.91 ± 0.38	0.05 ± 0.02	0.31 ± 0.43	-2.67 ± 0.63	-1.25 ± 0.93	-1.41 ± 0.85
	uLSW	0.22 ± 0.17	0.02 ± 0.01	-0.10 ± 0.40	-2.99 ± 0.53	-2.62 ± 0.69	-2.86 ± 0.68
	LSW	0.16 ± 0.12	0.01 ± 0.01	-0.04 ± 0.39	-2.85 ± 0.62	-3.17 ± 0.52	-2.72 ± 0.74
	ISOW	0.03 ± 0.05	0.00 ± 0.00	-0.13 ± 0.30	-2.38 ± 0.88	-2.97 ± 0.70	-2.48 ± 0.93
	DSOW	0.13 ± 0.12	-0.01 ± 0.00	-0.60 ± 0.18	-3.41 ± 0.62	-2.41 ± 0.87	-3.90 ± 0.66
Iceland	SPMW	1.15 ± 0.35	0.10 ± 0.02	0.61 ± 0.19	-4.14 ± 1.76	-2.32 ± 1.63	-2.27 ± 1.81
	uLSW	0.19 ± 0.08	0.01 ± 0.00	-0.24 ± 0.45	-2.08 ± 0.66	-2.31 ± 1.01	-2.12 ± 0.80
	LSW	-0.08 ± 0.05	0.00 ± 0.00	-0.04 ± 0.44	-2.26 ± 0.57	-2.26 ± 1.06	-2.38 ± 0.72
	ISOW	0.04 ± 0.10	0.01 ± 0.00	0.12 ± 0.40	-2.70 ± 0.43	-2.58 ± 0.99	-2.53 ± 0.60
Rockall	ENACW	1.13 ± 0.94	0.14 ± 0.04	0.73 ± 0.66	-2.25 ± 1.39	-0.58 ± 2.31	-0.25 ± 1.80
	SPMW	1.31 ± 0.29	0.10 ± 0.02	0.47 ± 0.22	-3.84 ± 1.23	-2.43 ± 1.90	-1.96 ± 1.28
	LSW	0.30 ± 0.24	0.01 ± 0.01	-0.14 ± 0.37	-0.94 ± 0.86	-1.36 ± 0.97	-0.76 ± 0.96

The increase in NC_T driven by the rise in C_{ant} was found to govern the acidification, with a contribution higher than the 67 % across the entire water column. The NC_T-driven pH_T decline was close to twice the observed and calculated acidification rates through the SPMW (Table 3). However, the contribution of NC_T at SPMW (67 %–69 %) was lower than that encountered toward the interior ocean (82 %–96 %) due to the relevance of temperature and A_T over pH_T trends in the upper layers. The cooling and increase in NA_T counteracted the acidification expected by the increasing C_T at SPMW by 28 %–34 % and 11 %–15 %, respectively. In the intermediate and deep layers, the thermal neutralization of the C_T-driven acidification was weaker (1.5 %–9.3 %) and the decreasing NA_T contributed to decreasing the pH_T by < 15 %. Freshening played a minor role in countering acidification (< 6 % in upper layers and < 2 % in the interior ocean).

In line with the declining pH_T, 79 %–83 % of the decrease in Ω in subsurface layers was attributed to the C_{ant}-driven rise in NC_T, with this influence reaching up to 97 % in deeper waters. The increase in NA_T in the SPMW accounted for 10.4 %–13.0 % in the trends and counteracted its NC_T-driven decrease by 12.6 %–16.2 %. The contribution of the NA_T fall and reversal toward deeper waters explained < 6 % of the decline in the uLSW, LSW, and ISOW in the Irminger basin and < 11 % in the Iceland basin. The pronounced impact of the rapid decrease in NA_T on the acidification of the DSOW (see Sect. 4.3) depicted the greater contribution of NA_T encountered in the Irminger basin (16 %) and compensated for the NC_T-driven decrease in Ω by 36.4 %. In the Rockall Trough, the contribution of NC_T changes was reduced in the LSW (78.2 %–79.0 %) compared to the Irminger basin (94.5 %), while the effect of NA_T fluctuations tripled until reaching 12.6 %–12.7 %.

Despite the crucial role of cooling in mitigating acidification, temperature fluctuations have the opposite effect on Ω due to the thermodynamic relationship inherent in the acid–base equilibrium of the CO_2–carbonate system (Dickson and Millero, 1987). In the Irminger and Iceland basins, the observed decrease in temperature contributed negligibly to the decline in Ω (3.6 % in the SPMW and less than 2 % in intermediate and deep waters). The influence of salinity, as with the pH_T trends, was minimal: the observed freshening slightly elevated the trends, offsetting the decline by 4.6 %–4.7 % in the SPMW, 1.1 %–2.1 % in the uLSW and LSW, and 0.5 %–1.2 % in the ISOW and DSOW. Even with the slightly faster cooling and freshening observed in the Rockall Trough, the contributions of temperature and salinity to Ω did not exceed 7 % in any of its layers.

5 Conclusions

This research has evaluated the interannual changes in the basin-wide MCS dynamics along the NASPG during 2009–2019. Despite the observational period being relatively short for quantifying long-term trends and formulating significant future projections, the findings have allowed us to evaluate the ocean response, in terms of MCS dynamics and on an interannual scale, to changes in deep-water convection and to isolate events affecting the physical patterns. The assessment of OA within the Irminger and Iceland basins was enhanced by supplying novel data and trends spanning 1 decade in which the physical patterns reversed. Additionally, the study

Table 4. Temporal changes in Ca and Arag (in 10^{-3} units yr^{-1}) explained by fluctuations in temperature ($\frac{\partial\Omega}{\partial T}\frac{\partial T}{dt}$), salinity ($\frac{\partial\Omega}{\partial S}\frac{\partial S}{dt}$), A_T($\frac{\partial\Omega}{\partial A_T}\frac{\partial NA_T}{dt}$), and C_T($\frac{\partial\Omega}{\partial C_T}\frac{\partial NC_T}{dt}$) in each of the layers considered for the Irminger, Iceland, and Rockall basins during the period 2009–2019. The sum of the changes explained by the individual drivers represents the calculated interannual Ω change ($\frac{d\Omega}{dt}$calculated), as detailed in Sect. 2.2.6. The observed interannual Ω trends ($\frac{d\Omega}{dt}$observed), shown in Fig. 6 and provided in Table 2, are also added to the table for comparison.

Basin	Layer		$\frac{\partial\Omega}{\partial T}\frac{\partial T}{dt}$	$\frac{\partial\Omega}{\partial S}\frac{\partial S}{dt}$	$\frac{\partial\Omega}{\partial A_T}\frac{\partial NA_T}{dt}$	$\frac{\partial\Omega}{\partial C_T}\frac{\partial NC_T}{dt}$	$\frac{d\Omega}{dt}$ (obs)	$\frac{d\Omega}{dt}$ (calculated)
Irminger	SPMW	Calcite	−0.57 ± 0.24	−0.43 ± 0.18	1.68 ± 2.37	−13.35 ± 3.14	−11.03 ± 5.57	−12.67 ± 3.94
		Aragonite	−0.49 ± 0.20	−0.29 ± 0.12	1.07 ± 1.50	−8.47 ± 1.99	−7.17 ± 3.46	−8.17 ± 2.50
	uLSW	Calcite	−0.17 ± 0.13	−0.12 ± 0.05	−0.46 ± 1.82	−12.61 ± 2.24	−8.28 ± 5.16	−13.36 ± 2.89
		Aragonite	−0.13 ± 0.10	−0.08 ± 0.03	−0.29 ± 1.16	−8.03 ± 1.43	−5.55 ± 3.21	−8.53 ± 1.84
	LSW	Calcite	−0.15 ± 0.11	−0.09 ± 0.05	−0.17 ± 1.55	−10.42 ± 2.27	−13.54 ± 2.88	−10.83 ± 2.75
		Aragonite	−0.11 ± 0.08	−0.06 ± 0.03	−0.11 ± 0.99	−6.69 ± 1.45	−8.65 ± 1.83	−6.97 ± 1.76
	ISOW	Calcite	−0.04 ± 0.05	0.00 ± 0.01	−0.44 ± 1.03	−7.48 ± 2.75	−10.35 ± 3.23	−7.96 ± 2.94
		Aragonite	−0.02 ± 0.04	0.00 ± 0.01	−0.29 ± 0.67	−4.84 ± 1.78	−6.66 ± 2.04	−5.15 ± 1.90
	DSOW	Calcite	−0.13 ± 0.12	0.03 ± 0.02	−1.78 ± 0.52	−9.23 ± 1.68	−4.30 ± 2.76	−11.11 ± 1.77
		Aragonite	−0.09 ± 0.09	0.02 ± 0.01	−1.16 ± 0.34	−6.01 ± 1.10	−3.02 ± 1.68	−7.24 ± 1.15
Iceland	SPMW	Calcite	−0.88 ± 0.26	−0.86 ± 0.16	3.16 ± 1.00	−19.59 ± 8.35	−15.77 ± 10.40	−18.17 ± 8.42
		Aragonite	−0.72 ± 0.22	−0.58 ± 0.10	2.02 ± 0.64	−12.48 ± 5.32	−10.37 ± 6.55	−11.77 ± 5.37
	uLSW	Calcite	−0.17 ± 0.07	−0.09 ± 0.03	−1.02 ± 1.89	−7.98 ± 2.52	−9.18 ± 5.11	−9.26 ± 3.15
		Aragonite	−0.12 ± 0.05	−0.06 ± 0.02	−0.65 ± 1.21	−5.11 ± 1.61	−5.92 ± 3.23	−5.95 ± 2.02
	LSW	Calcite	0.08 ± 0.05	0.02 ± 0.01	−0.15 ± 1.70	−7.92 ± 2.00	−7.53 ± 4.64	−7.97 ± 2.63
		Aragonite	0.06 ± 0.03	0.01 ± 0.01	−0.09 ± 1.09	−5.10 ± 1.29	−4.83 ± 2.96	−5.12 ± 1.69
	ISOW	Calcite	−0.04 ± 0.10	−0.03 ± 0.02	0.41 ± 1.37	−8.38 ± 1.33	−7.22 ± 4.34	−8.05 ± 1.91
		Aragonite	−0.03 ± 0.07	−0.02 ± 0.01	0.27 ± 0.89	−5.43 ± 0.86	−4.72 ± 2.76	−5.22 ± 1.24
Rockall	ENACW	Calcite	−0.82 ± 0.69	−1.50 ± 0.38	5.16 ± 4.63	−14.21 ± 8.78	−11.60 ± 12.67	−11.37 ± 9.95
		Aragonite	−0.79 ± 0.66	−1.00 ± 0.25	3.29 ± 2.95	−9.06 ± 5.60	−7.66 ± 7.96	−7.57 ± 6.37
	SPMW	Calcite	−1.15 ± 0.26	−0.82 ± 0.18	2.44 ± 1.15	−18.21 ± 5.83	−20.57 ± 13.40	−17.74 ± 5.95
		Aragonite	−0.93 ± 0.21	−0.55 ± 0.12	1.56 ± 0.74	−11.66 ± 3.73	−13.24 ± 8.47	−11.58 ± 3.81
	LSW	Calcite	−0.28 ± 0.22	−0.10 ± 0.08	−0.58 ± 1.57	−3.62 ± 3.30	−7.88 ± 4.41	−4.59 ± 3.66
		Aragonite	−0.21 ± 0.16	−0.07 ± 0.05	−0.37 ± 1.01	−2.33 ± 2.12	−4.97 ± 2.82	−2.97 ± 2.35

provides an unprecedented analysis of the physicochemical variations in the Rockall Trough, which is crucial for the assessment of the entire longitudinal span of the NASPG. It facilitates a more accurate understanding of the mechanisms dictating basin-scale acidification processes and advances our understanding of OA in the North Atlantic and the global ocean.

Overall, the entrance and accumulation of C_{ant} and interannual acidification trends were strongly affected by the cooling, freshening, and enhancement in the oxygenation during this decade. The longitudinal span of the NASPG and the differences in circulation patterns, water masses, and bathymetry behaved as a source of spatiotemporal variability. The interannual acidification trends of the main water masses across the NASPG ranged between 0.0006–0.0032 units yr^{-1} and caused a decline in the ΩCa and ΩArag of 0.004–0.021 and 0.003–0.013 units yr^{-1}, respectively. The convective processes increased the accumulation rates of C_{ant} in the interior ocean by 50 %–86 % and accelerated the acidification rates by around 10 % compared to previous decades in the Irminger and Iceland basins. The shallower hydrography of the Rockall Trough and the poleward circulation patterns accounted for differences in the acidification rates with respect to the surrounding waters.

The C_{ant}-driven increase in NC_T was found to govern the acidification of the NASPG, with contributions exceeding 60 %. The combined effect of the decreasing temperature, salinity, and NA_T neutralized close to one-half of the acidification along the entire longitudinal span of the SPMW. The enhanced deep-water ventilation in the western NASPG slowed down the cooling and freshening toward the interior ocean, weakening the physical counterbalance of acidification.

The present investigation emphasizes the progressive increase in the uptake and accumulation of C_{ant} and the subsequent acceleration in OA along the NASPG. Novel data and results provided could be compared with other repeated hydrographic section data at mid- and high latitudes in the North Atlantic, such as the A02, A25, AR07E, and AR28 framed in the GO-SHIP programme, and are used in conjunction to develop future investigations. Additionally, they contribute to the improvement of the projections pertaining to the future state of the oceans run by models and forecasts. Considering the important variability in the mechanism controlling the distribution of the physico-biogeochemical properties and particularly the OA in the North Atlantic, this research aims to highlight the necessity of continuing to monitor and sample the whole water column through repeated hydrographic sections, especially through the highly variable but less assessed easternmost part.

Appendix A: Correction of dissolved oxygen records for the cruise of 2019

The sensor-measured DO data for the cruise of 2019 were corrected by considering the DO output data given by the neural network ESPER_NN (Carter et al., 2021) for the cruises of 2016 and 2019 (hereinafter ESPER-estimated DO) and the Winkler-measured DO during the cruise of 2016. Among the 16 equations provided by the ESPER_NN, which differently combine seawater properties as predictors, we use Eq. (8), which only needs the T and S an inputs (due to lack of measured macronutrients during the cruise of 2019), along with latitude, longitude, depth, and date (see Table 2 in Carter et al., 2021). The reported root-mean-square error (RMSE) of Eq. (8) for DO estimations in the global ocean is $\pm 9.7\,\mu\mathrm{mol\,kg^{-1}}$, which is reduced for intermediate waters (1000–1500 m) to $\pm 5.9\,\mu\mathrm{mol\,kg^{-1}}$ (see Table 7 in Carter et al., 2021). Additionally, a new set of DO for 2019 based on Winkler data for 2016 was computed, which was referred to in this study as "pseudo-Winkler" data. The difference between Winkler-measured and ESPER-estimated DO during 2016 was interpolated to the longitudes and depths of the samples of 2019 by applying Delaunay triangulation. The pseudo-Winkler data were described as the sum of these interpolated differences and the ESPER-estimated DO data for 2019. The longitudinal distribution of measured and ESPER-estimated DO data for 2016 and 2019 is depicted in Figs. S1a and S1b. The interpolated pseudo-Winkler data for the cruise of 2019 are included in Fig. S1a.

The sensor records of DO in 2019 were on average $4.90\,\mu\mathrm{mol\,kg^{-1}}$ lower than the ESPER-estimated and $10.31\,\mu\mathrm{mol\,kg^{-1}}$ lower than the pseudo-Winkler. A higher discrepancy was observed in the average sensor-measured DO in the eastern part ($237.60 \pm 15.00\,\mu\mathrm{mol\,kg^{-1}}$) compared with the western part ($281.40 \pm 14.75\,\mu\mathrm{mol\,kg^{-1}}$). The average differences (measured minus ESPER-estimated DO and measured minus pseudo-Winkler DO, $\Delta\mathrm{DO_{meas\text{-}ESPER}}$ and $\Delta\mathrm{DO_{meas\text{-}pseudoWinkler}}$, respectively; Figs. S2c and S1d) show that the sensor records were strongly underestimated in the eastern part (-20.98 ± 10.91 and $-28.77 \pm 12.60\,\mu\mathrm{mol\,kg^{-1}}$, respectively) and weakly overestimated in the western part (8.59 ± 8.53 and $5.18 \pm 12.02\,\mu\mathrm{mol\,kg^{-1}}$, respectively) during the cruise of 2019. These differences were corrected separately west and east of 21.5° W by using the relationship $\frac{\Delta\mathrm{DO_{meas\text{-}pseudoWinkler}}}{\mathrm{measured\,DO}}$. The averages of this relationship in the western and eastern parts of the transect (0.016 and $-0.12\,\mu\mathrm{mol\,kg^{-1}}$, respectively) were used as corrector factors. The corrected DO values were given by the product of the measured DO and $\left(1 - \frac{\Delta\mathrm{DO_{meas\text{-}pseudoWinkler}}}{\mathrm{measured\,DO}}\right)$.

Appendix B: Interannual trends in A_T and $\mathrm{NA_T}$

The interannual trends in A_T (Fig. S4 and Table S4) were found to be highly impacted by freshening, with decreasing rates ranging from -0.33 to $-0.71\,\mu\mathrm{mol\,kg^{-1}\,yr^{-1}}$ among the SPMW and ENACW and from -0.01 to $-0.18\,\mu\mathrm{mol\,kg^{-1}\,yr^{-1}}$ within the uLSW, LSW, ISOW, and DSOW. It contrasts with the minimal interannual changes and slight rates of increase in A_T encountered among the different layers by García-Ibáñez et al. (2016) from 1991 to 2015 in the Irminger basin (between 0.10 and $0.28\,\mu\mathrm{mol\,kg^{-1}\,yr^{-1}}$) and in the Iceland basin (between -0.04 and $0.07\,\mu\mathrm{mol\,kg^{-1}\,yr^{-1}}$) and with the trends reported for the period 1983–2013 by Pérez et al. (2021) at the IRM-TS (between 0.13 and $0.22\,\mu\mathrm{mol\,kg^{-1}\,yr^{-1}}$) and at the IS-TS (between -0.04 and $0.15\,\mu\mathrm{mol\,kg^{-1}\,yr^{-1}}$). These heterogeneities in the temporal evolution of the A_T were driven by the decadal salinification of the whole water column observed since the late 20th century and interrupted by interannual freshening episodes such as during the 2010s.

The interannual increase in $\mathrm{NA_T}$ in upper layers could be related to acidification, which favours the dissolution of carbonates, combined with increasing biological production reported for upper layers across the NASPG (Ostle et al, 2022). It contrasts with the constantly weak decrease in $\mathrm{NA_T}$ in intermediate and deep layers, in which the accelerated acidification was compensated by the dominance of remineralization processes over lower biological uptake. Consequently, the positive $\mathrm{NA_T}$ trends encountered in the upper layers led to a rise in $\mathrm{pH_T}$, while the diminished $\mathrm{NA_T}$ contributed to decreasing the $\mathrm{pH_T}$ toward the interior ocean.

The A_T/S relationship has increased at a rate of $0.5 \pm 0.2\,\mu\mathrm{mol\,kg^{-1}\,yr^{-1}}$ (p-value < 0.05) due to the combined action of the freshening (Fig. 4) and the progressive increase in A_T-rich water inflows through upper layers (observed in the positive trends in $\mathrm{NA_T}$ in SPMW and ENACW; Fig. S4). This was likely associated with the stagnation of A_T-rich subtropical waters in the upper layers due to the slowdown of the NASPG since the mid-1990s (e.g. Böning et al., 2006; Häkkinen and Rhines, 2004), along with changes in the spreading of waters from higher latitudes influenced by melting.

Code availability. The MATLAB and R codes for CANYONB (Bittig et al., 2018) are available at https://github.com/HCBScienceProducts/CANYON-B (last access: 9 December 2024). The MATLAB and R codes for ESPER_NN (Carter et al., 2021) are available at https://github.com/BRCScienceProducts/ESPER (last access: 9 December 2024). The anthropogenic carbon calculation (Pérez et al., 2008; Vázquez-Rodríguez et al., 2009) was run using the MATLAB code developed by the Oceanology group at the IIM-CSIC available at http://oceano.iim.csic.es/co2group (last access: 9 December 2024; Oceanology group, 2016). The CO2SYS programme for MATLAB (van Heuven et al., 2011; Orr et al., 2018; Sharp et al., 2023) is available at https://github.com/jonathansharp/CO2-System-ExtdTS29 (last access: 9 December 2024).

Data availability. The measured surface-to-bottom CLIVAR data (2009–2019) used in this investigation are published at Zenodo (https://doi.org/10.5281/zenodo.10276221; Santana-Casiano et al., 2023). The GO-SHIP A25-OVIDE data for the cruise of 2018 are available at SEANOE (https://www.seanoe.org/data/00762/87394/, Lherminier et al., 2022).

Supplement. The supplement related to this article is available online at: https://doi.org/10.5194/bg-21-5561-2024-supplement.

Author contributions. DCH contributed to data analysis and wrote the article. FFP, DCH, AV, DGS, AGG, MGD, and JMSC worked on the design, conceptualization, and data preparation. SG, AS, MGD, JMSC, AGG, and DGS participated in eight, four, seven, seven, two, and two cruises, respectively. SG and AS were the chief scientists on all cruises and were responsible for the operational and maintenance procedures for the CTD and additional sensors and thus for physical and sensor-measured variables. MGD and JMSC acquired funding from the ULPGC to provide resources for the Spanish team. SG and AS acquired the funding for ship time and the provision of resources for all cruise participants. All authors critically reviewed the article.

Competing interests. The contact author has declared that none of the authors has any competing interests.

Disclaimer. Publisher's note: Copernicus Publications remains neutral with regard to jurisdictional claims made in the text, published maps, institutional affiliations, or any other geographical representation in this paper. While Copernicus Publications makes every effort to include appropriate place names, the final responsibility lies with the authors.

Acknowledgements. The participation on the cruises for the Spanish team from the ULPGC was funded by the Spanish Ministry of Science under the Complementary Actions CTM2008-05255, CTM2010-09514-E, and CTM2011-12984-E (years 2009–2011); by the FP7 European project CARBOCHANGE under grant agreement no. 264879; and by the Spanish Innovation and Science Ministry through projects EACFe (CTM2014-52342-P) and ATOPFe (CTM2017-83476-P). Sergey V. Gladyshev and Alexey Sokov were supported by FMWE-2023-0002. Fiz F. Pérez and Antón Velo were supported by the BOCATS2 (PID2019-104279GB-C21) project funded by MCIN/AEI/10.13039/501100011033 and by the EuroGO-SHIP project (Horizon Europe #101094690). The participation of David Curbelo-Hernández was funded by the PhD grant PIFULPGC-2020-2 ARTHUM-2. We thank the technician and researchers Adrian Castro Álamo (two cruises), Anna Barrera Galderique (three cruises), Rayco Alvarado Medina (two cruises), and Pilar Aparicio Rizzo (one cruise) who helped with in situ analysis. We also thank the technicians at the P. P. Shirshov Institute of Oceanology of the Russian Academy of Science for the in situ analysis of dissolved oxygen and nutrients.

Financial support. This research has been supported by the Ministerio de Ciencia e Innovación (grant nos. CTM2008-05255, CTM2010-09514-E, CTM2011-12984-E, CTM2014-52342-P, CTM2017-83476-P, and PID2019-104279GB-C21); the HORIZON EUROPE Research Infrastructures (grant no. 101094690); the Universidad de Las Palmas de Gran Canaria (grant no. PIFULPGC-2020-2 ARTHUM-2); and the Shirshov Institute of Oceanology, Russian Academy of Sciences (grant no. FMWE-2023-0002).

Review statement. This paper was edited by Frédéric Gazeau and reviewed by two anonymous referees.

References

Accornero, A., Manno, C., Esposito, F., and Gambi, M. C.: The vertical flux of particulate matter in the polynya of Terra Nova Bay, Part II. Biological components, Antarct. Sci., 15, 175–188, https://doi.org/10.1017/S0954102003001214, 2003.

Álvarez, M., Ríos, A. F., Pérez, F. F., Bryden, H. L., and Rosón, G.: Transports and budgets of total inorganic carbon in the subpolar and temperate North Atlantic, Global Biogeochem. Cy., 17, 1002, https://doi.org/10.1029/2002gb001881, 2003.

Álvarez, M., Pérez, F. F., Bryden, H., and Ríos, A. F.: Physical and biogeochemical transports structure in the North Atlantic subpolar gyre, J. Geophys. Res.-Ocean., 109, C03027, https://doi.org/10.1029/2003jc002015, 2004.

Azetsu-Scott, K., Jones, E. P., Yashayaev, I., and Gershey, R. M.: Time series study of CFC concentrations in the Labrador Sea during deep and shallow convection regimes (1991–2000), J. Geophys. Res.-Ocean., 108, 354, https://doi.org/10.1029/2002JC001317, 2003.

Balmaseda, M. A., Smith, G. C., Haines, K., Anderson, D., Palmer, T. N., and Vidard, A.: Historical reconstruction of the Atlantic Meridional Overturning Circulation from the ECMWF operational ocean reanalysis, Geophys. Res. Lett., 34, 1–6, https://doi.org/10.1029/2007GL031645, 2007.

Bates, N. R., Best, M. H. P., Neely, K., Garley, R., Dickson, A. G., and Johnson, R. J.: Detecting anthropogenic carbon dioxide uptake and ocean acidification in the North Atlantic Ocean, Biogeosciences, 9, 2509–2522, https://doi.org/10.5194/bg-9-2509-2012, 2012.

Bates, N. R., Astor, Y. M., Church, M. J., Currie, K., Dore, J. E., González-Dávila, M., Lorenzoni, L., Muller-Karger, F., Olafsson, J., and Santana-Casiano, J. M.: A time-series view of changing surface ocean chemistry due to ocean uptake of anthropogenic CO_2 and ocean acidification, Oceanography, 27, 126–141, https://doi.org/10.5670/oceanog.2014.16, 2014.

Bathmann, U. V., Noji, T. T., and von Bodungen, B.: Sedimentation of pteropods in the Norwegian Sea in autumn, Deep-Sea Res. Pt. A, 38, 1341–1360, https://doi.org/10.1016/0198-0149(91)90031-A, 1991.

Bellerby, R. G., Olsen, A., Furevik, T., and Anderson, L. G.: Response of the surface ocean CO_2 system in the Nordic Seas and Northern North Atlantic to climate change, Geophys. Monogr. Ser., 158, 189–197, https://doi.org/10.1029/158GM13, 2005

Benson, B. B. and Krause, D.: The concentration and isotopic fractionation of oxygen dissolved in freshwater and seawater in equilibrium with the atmosphere, Deep-Sea Res. Pt. B, 31, 859, https://doi.org/10.1016/0198-0254(84)93289-8, 1984.

Bersch, M., Yashayaev, I., and Koltermann, K. P.: Recent changes of the thermohaline circulation in the subpolar North Atlantic, Ocean Dynam., 57, 223–235, 2007.

Bittig, H. C., Steinhoff, T., Claustre, H., Fiedler, B., Williams, N. L., Sauzède, R., Körtzinger, A., and Gattuso, J. P.: An alternative to static climatologies: Robust estimation of open ocean CO_2 variables and nutrient concentrations from T, S, and O_2 data using Bayesian neural networks, Front. Mar. Sci., 5, 1–29, https://doi.org/10.3389/fmars.2018.00328, 2018.

Böning, C. W., Scheinert, M., Dengg, J., Biastoch, A., and Funk, A.: Decadal variability of subpolar gyre transport and its reverberation in the North Atlantic overturning, Geophys. Res. Lett., 33, L21S01, https://doi.org/10.1029/2006GL026906, 2006.

Brambilla, E. and Talley, L. D.: Subpolar mode water in the northeastern Atlantic: 1. Averaged properties and mean circulation, J. Geophys. Res.-Ocean., 113, 1–18, https://doi.org/10.1029/2006JC004062, 2008.

Broecker, W. S. and Peng, T. H.: Tracers in the Sea: W. S. Broecker and T. H. Peng, Geochim. Cosmochim. Ac., 47, 1336, https://doi.org/10.1016/0016-7037(83)90075-3, 1983.

Caldeira, K. and Wickett, M. E.: Anthropogenic carbon and ocean pH, Nature, 425, 365, https://doi.org/10.1038/425365a, 2003.

Caldeira, K. and Wickett, M. E.: Ocean model predictions of chemistry changes from carbon dioxide emissions to the atmosphere and ocean, J. Geophys. Res.-Ocean., 110, 1–12, https://doi.org/10.1029/2004JC002671, 2005.

Carpenter, J. H.: The accuracy of the Winkler method for dissolved oxygen analysis, Limnol. Oceanogr., 10, 135–140, 1965.

Carrit, D. E. and Carpenter, J. H.: Recommendation procedure for Winkler analyses of sea water for dissolved oxygen, J. Mar. Res., 24, 313–318, 1966.

Carter, B. R., Bittig, H. C., Fassbender, A. J., Sharp, J. D., Takeshita, Y., Xu, Y. Y., Álvarez, M., Wanninkhof, R., Feely, R. A., and Barbero, L.: New and updated global empirical seawater property estimation routines, Limnol. Oceanogr. Method., 19, 785–809, https://doi.org/10.1002/lom3.10461, 2021.

Chau, T.-T.-T., Gehlen, M., Metzl, N., and Chevallier, F.: CMEMS-LSCE: a global, 0.25°, monthly reconstruction of the surface ocean carbonate system, Earth Syst. Sci. Data, 16, 121–160, https://doi.org/10.5194/essd-16-121-2024, 2024.

Clayton, T. D. and Byrne, R. H.: Spectrophotometric seawater pH measurements: Total hydrogen ion concentration scale calibration of m-cresol purple and at-sea results, Deep-Sea Res. Pt. I, 40, 2115–2129, https://doi.org/10.1016/0967-0637(93)90048-8, 1993.

Collier, R., Dymond, J., Honjo, S., Manganini, S., François, R., and Dunbar, R.: The vertical flux of biogenic and lithogenic material in the Ross Sea: Moored sediment trap observations 1996–1998, Deep-Sea Res. Pt. II, 47, 3491–3520, https://doi.org/10.1016/S0967-0645(00)00076-X, 2000.

Corbière, A., Metzl, N., Reverdin, G., Brunet, C., and Takahashi, T.: Interannual and decadal variability of the oceanic carbon sink in the North Atlantic subpolar gyre, Tellus B, 59, 168–178, https://doi.org/10.1111/j.1600-0889.2006.00232.x, 2007.

Daniault, N., Mercier, H., Lherminier, P., Sarafanov, A., Falina, A., Zunino, P., Pérez, F. F., and Ríos, A. F.: The northern North Atlantic Ocean mean circulation in the early 21st century, Prog. Oceanogr., 146, 142–158, https://doi.org/10.1016/j.pocean.2016.06.007, 2016.

de Jong, M. F. and de Steur, L.: Strong winter cooling over the Irminger Sea in winter 2014–2015, exceptional deep convection, and the emergence of anomalously low SST, Geophys. Res. Lett., 43, 7106–7113, https://doi.org/10.1002/2016GL069596, 2016.

de Jong, M. F., van Aken, H. M., Våge, K., and Pickart, R. S.: Convective mixing in the central Irminger Sea: 2002–2010, Deep-Sea Res. Pt. I, 63, 36–51, https://doi.org/10.1016/j.dsr.2012.01.003, 2012.

de la Paz, M., García-Ibáñez, M. I., Steinfeldt, R., Ríos, A. F., and Pérez, F. F.: Ventilation versus biology: What is the controlling mechanism of nitrous oxide distribution in the North Atlantic?, Global Biogeochem. Cy., 31, 745–760, https://doi.org/10.1002/2016GB005507, 2017.

DelValls, T. A. and Dickson, A. G.: The pH of buffers based on 2-amino-2-hydroxymethyl-1,3-propanediol ("tris") in synthetic sea water, Deep-Sea Res. Pt. I, 45, 1541–1554, https://doi.org/10.1016/S0967-0637(98)00019-3, 1998.

Desbruyères, D., Thierry, V., and Mercier, H.: Simulated decadal variability of the meridional overturning circulation across the A25-Ovide section, J. Geophys. Res.-Ocean., 118, 462–475, https://doi.org/10.1029/2012JC008342, 2013.

Dickson, A. D.: Determination of dissolved oxygen in sea water by Winkler titration. WOCE Operations Manual, Part 3.1.3 Operations and Methods, WHP Office Report WHPO 91-1, 1995.

Dickson, A. G.: Standard potential of the reaction: $AgCl(s) + 1/2H2(g) = Ag(s) + HCl(aq)$, and the standard acidity constant of the ion HSO_4 in synthetic sea water from 273.15 to 318.15 K, J. Chem. Thermodyn., 22, 113–127, https://doi.org/10.1016/0021-9614(90)90074-Z, 1990.

Dickson, A. G. and Goyet, C.: Handbook of methods for the analysis of the various parameters of the carbon dioxide system in sea water, Version 2, Oak Ridge, TN, Oak Ridge National Lab, (ORNL), 198 pp., (ORNL/CDIAC-74), https://doi.org/10.2172/10107773, 1994.

Dickson, A. G. and Millero, F. J.: A comparison of the equilibrium constants for the dissociation of carbonic acid in seawater media, Deep-Sea Res. Pt. A, 34, 1733–1743, https://doi.org/10.1016/0198-0149(87)90021-5, 1987.

Dickson, A. G., Sabine, C. L., and Christian, J. R. (Eds.): Guide to best practices for ocean CO_2 measurements, PICES Spec. Publ., 3, 191 pp., ISBN: 1-897176-07-4, 2007.

Dickson, B., Yashayaev, I., Meincke, J., Turrell, B., Dye, S., and Holfort, J.: Rapid freshening of the deep North Atlantic Ocean over the past four decades, Nature, 416, 832–837, https://doi.org/10.1038/416832a, 2002.

Dickson, R. R. and Brown, J.: The production of North Atlantic Deep Water: Sources, rates, and pathways, J. Geophys. Res.-Ocean., 99, 12319–12341, https://doi.org/10.1029/94JC00530, 1994.

Doney, S. C., Fabry, V. J., Feely, R. A., and Kleypas, J. A.: Ocean acidification: The other CO_2 problem, Annu. Rev. Mar. Sci., 1, 169–192, https://doi.org/10.1146/annurev.marine.010908.163834, 2009.

Eden, C. and Willebrand, J.: Mechanism of interannual to decadal variability of the North Atlantic circulation, J. Clim., 14, 2266–2280, https://doi.org/10.1175/1520-0442(2001)014<2266>2.0.CO;2, 2001.

Ellett, D. J., Edwards, A., and Bowers, R.: The hydrography of the Rockall Channel – an overview, Proc. R. Soc. Edinb. Sect. B, 88, 61–81, https://doi.org/10.1017/s0269727000004474, 1986.

Feely, R. A., Sabine, C. L., Lee, K., Berelson, W., Kleypas, J., Fabry, V. J., and Millero, F. J.: Impact of anthropogenic CO_2 on the $CaCO_3$ system in the oceans, Science, 305, 362–366, https://doi.org/10.1126/SCIENCE.1097329, 2004.

Feely, R. A., Doney, S. C., and Cooley, S. R.: Ocean acidification: Present conditions and future changes in a high-CO_2 world, Oceanography, 22, 36–47, https://www.jstor.org/stable/24861022 (last access: 9 December 2024), 2009.

Ferron, B., Kokoszka, F., Mercier, H., and Lherminier, P.: Dissipation rate estimates from microstructure and finescale internal wave observations along the A25 Greenland–Portugal OVIDE line, J. Atmos. Ocean. Technol., 31, 2530–2543, https://doi.org/10.1175/JTECH-D-14-00036.1, 2014.

Fogelqvist, E., Blindheim, J., Tanhua, T., Østerhus, S., Buch, E., and Rey, F.: Greenland–Scotland overflow studied by hydro-chemical multivariate analysis, Deep-Sea Res. Pt. I, 50, 73–102, 2003.

Fontela, M., Pérez, F. F., Carracedo, L. I., Padín, X. A., Velo, A., García-Ibañez, M. I., and Lherminier, P.: The Northeast Atlantic is running out of excess carbonate in the horizon of cold-water corals communities, Sci. Rep., 10, 14714, https://doi.org/10.1038/s41598-020-71793-2, 2020.

Friedlingstein, P., O'Sullivan, M., Jones, M. W., Andrew, R. M., Gregor, L., Hauck, J., Le Quéré, C., Luijkx, I. T., Olsen, A., Peters, G. P., and Peters, W.: Global Carbon Budget 2022, Earth Syst. Sci. Data, 14, 4811–4900, https://doi.org/10.5194/essd-14-4811-2022, 2022.

Fröb, F., Olsen, A., Becker, M., Chafik, L., Johannessen, T., Reverdin, G., and Omar, A.: Wintertime fCO_2 variability in the subpolar North Atlantic since 2004, Geophys. Res. Lett., 46, 1580–1590, https://doi.org/10.1029/2018

García-Ibáñez, M. I., Pardo, P. C., Carracedo, L. I., Mercier, H., Lherminier, P., Ríos, A. F., and Pérez, F. F.: Structure, transports and transformations of the water masses in the Atlantic Subpolar Gyre, Prog. Oceanogr., 135, 18–36, https://doi.org/10.1016/j.pocean.2015.03.009, 2015.

García-Ibáñez, M. I., Zunino, P., Fröb, F., Carracedo, L. I., Ríos, A. F., Mercier, H., Olsen, A., and Pérez, F. F.: Ocean acidification in the subpolar North Atlantic: Rates and mechanisms controlling pH changes, Biogeosciences, 13, 3701–3715, https://doi.org/10.5194/bg-13-3701-2016, 2016.

García-Ibáñez, M. I., Pérez, F. F., Lherminier, P., Zunino, P., Mercier, H., and Tréguer, P.: Water mass distributions and transports for the 2014 GEOVIDE cruise in the North Atlantic, Biogeosciences, 15, 2075–2090, https://doi.org/10.5194/bg-15-2075-2018, 2018.

García-Ibáñez, M. I., Bates, N. R., Bakker, D. C. E., Fontela, M., and Velo, A.: Cold-water corals in the Subpolar North Atlantic Ocean exposed to aragonite undersaturation if the 2 °C global warming target is not met, Glob. Planet. Change, 201, 103480, https://doi.org/10.1016/j.gloplacha.2021.103480, 2021.

Gattuso, J. P., Magnan, A., Billé, R., Cheung, W. W. L., Howes, E. L., Joos, F., Allemand, D., Bopp, L., Cooley, S. R., Eakin, C. M., Hoegh-Guldberg, O., Kelly, R. P., Pörtner, H. O., Rogers, A. D., Baxter, J. M., Laffoley, D., Osborn, D., Rankovic, A., Rochette, J., Sumaila, U. R., Treyer, S., and Turley, C.: Contrasting futures for ocean and society from different anthropogenic CO_2 emissions scenarios, Science, 349, 6243, https://doi.org/10.1126/science.aac4722, 2015.

Gehlen, M., Séférian, R., Jones, D. O. B., Roy, T., Roth, R., Barry, J., Bopp, L., Doney, S. C., Dunne, J. P., Heinze, C., Joos, F., Orr, J. C., Resplandy, L., Segschneider, J., and Tjiputra, J.: Projected pH reductions by 2100 might put deep North Atlantic biodiversity at risk, Biogeosciences, 11, 6955–6967, https://doi.org/10.5194/bg-11-6955-2014, 2014.

Gladyshev, S. V., Gladyshev, V. S., and Falina, A. S.: Winter convection in the Irminger Sea in 2004–2014, Oceanology, 56, 326–335, https://doi.org/10.1134/S0001437016030073, 2016a.

Gladyshev, S. V., Gladyshev, V. S., and Gulev, S. K.: Anomalously deep convection in the Irminger Sea during the winter of 2014–2015, Dokl. Earth Sci., 469, 766–770, https://doi.org/10.1134/S1028334X16070229, 2016b.

Gladyshev, S. V., Gladyshev, V. S., Member, C., Gulev, R. A. S. S. K., and Sokov, A. V.: Subpolar Mode Water Classes in the Northeast Atlantic: Interannual and Long-Term Variability, Dokl. Earth Sci., 476, 1203–1206, https://doi.org/10.1134/S1028334X17100166, 2017.

Gladyshev, S. V., Gladyshev, V. S., Member, C., Gulev, R. A S. S. K., and Sokov, A. V.: Structure and Variability of the Meridional Overturning Circulation in the North Atlantic Subpolar Gyre, 2007–2017, Dokl. Earth Sci., 483, 1524–1527, https://doi.org/10.1134/S1028334X18120024, 2018.

González-Dávila, M. and Santana-Casiano, J. M.: Long-term trends of pH and inorganic carbon in the Eastern North Atlantic: The ESTOC site, Front. Mar. Sci., 10, 1236214, https://doi.org/10.3389/fmars.2023.1236214, 2023.

González-Dávila, M., Santana-Casiano, J. M., Rueda, M. J., and Llinás, O.: The water column distribution of carbonate system variables at the ESTOC site from 1995 to 2004, Biogeosciences, 7, 3067–3081, https://doi.org/10.5194/bg-7-3067-2010, 2010.

González-Dávila, M., Santana-Casiano, J. M., and Prêcheur-Massieu, H.: New pH sensor for monitoring ocean acidification, Sea Technol., 55, 36–40, 2014.

González-Dávila, M., Santana-Casiano, J. M., Petihakis, G., Ntoumas, M., Suárez de Tangil, M., and Krasakopoulou, E.: Seasonal pH variability in the Saronikos Gulf: A year-study using a new photometric pH sensor, J. Mar. Syst., 162, 37–46, https://doi.org/10.1016/j.jmarsys.2016.03.007, 2016.

Gruber, N., Sarmiento, J. L., and Stocker, T. F.: An improved method for detecting anthropogenic CO_2 in the oceans, Global Biogeochem. Cy., 10, 809–837, https://doi.org/10.1029/96GB01608, 1996.

Gruber, N., Clement, D., Carter, B. R., Feely, R. A., van Heuven, S., Hoppema, M., Ishii, M., Key, R. M., Kozyr, A., Lauvset, S. K., Monaco, C. Lo, Mathis, J. T., Murata, A., Olsen, A., Perez, F. F., Sabine, C. L., Tanhua, T., and Wanninkhof, R.: The oceanic sink for anthropogenic CO_2 from 1994 to 2007, Science, 363, 1193–1199, https://doi.org/10.1126/science.aau5153, 2019.

Guallart, E. F., Fajar, N. M., Padín, X. A., Vázquez-Rodríguez, M., Calvo, E., Ríos, A. F., Hernández-Guerra, A., Pelejero, C., and Pérez, F. F.: Ocean acidification along the 24.5° N section in the subtropical North Atlantic, Geophys. Res. Lett., 42, 450–458, https://doi.org/10.1002/2014GL062971, 2015.

Guinotte, J. M., Orr, J., Cairns, S., Freiwald, A., Morgan, L., and George, R.: Will human-induced changes in seawater chemistry alter the distribution of deep-sea scleractinian corals?, Front. Ecol. Environ., 4, 141–146, https://doi.org/10.1890/1540-9295(2006)004[0141:WHCISC]2.0.CO;2, 2006.

Häkkinen, S. and Rhines, P. B.: Decline of Subpolar North Atlantic Circulation during the 1990s, Science, 304, 555–559, https://doi.org/10.1126/science.1094917, 2004.

Harvey, J.: Θ-S relationships and water masses in the eastern North Atlantic, Deep-Sea Res. Pt. A, 29, 1021–1033, https://doi.org/10.1016/0198-0149(82)90025-5, 1982.

Hátún, H., Sande, A. B., Drange, H., Hansen, B., and Valdimarsson, H.: Influence of the Atlantic subpolar gyre on the thermohaline circulation, Science, 309, 1841–1844, https://doi.org/10.1126/science.1114777, 2005.

Holliday, N. P., Bersch, M., Berx, B., Chafik, L., Cunningham, S., Florindo-López, C., Hátún, H., Johns, W., Josey, S. A., Larsen, K. M. H., Mulet, S., Oltmanns, M., Reverdin, G., Rossby, T., Thierry, V., Valdimarsson, H., and Yashayaev, I.: Ocean circulation causes the largest freshening event for 120 years in eastern subpolar North Atlantic, Nat. Commun., 11, 585, https://doi.org/10.1038/s41467-020-14474-y, 2020.

Holliday, P. N., Pollard, R. T., Read, J. F., and Leach, H.: Water mass properties and fluxes in the Rockall Trough, 1975–1998, Deep-Sea Res. Pt. I, 47, 1303–1332, https://doi.org/10.1016/S0967-0637(99)00109-0, 2000.

Humphreys, M. P., Griffiths, A. M., Achterberg, E. P., Holliday, N. P., Rérolle, V. M. C., Menzel-Barraqueta, J.-L., Couldrey, M. P., Oliver, K. I. C., Hartman, S. E., Esposito, M., and Boyce, A. J.: Multidecadal accumulation of anthropogenic and remineralized dissolved inorganic carbon along the Extended Ellett Line in the northeast Atlantic Ocean, Global Biogeochem. Cy., 30, 293–310, https://doi.org/10.1002/2015GB005246, 2016.

IPCC: Climate Change 2013: The Physical Science Basis. Contribution of Working Group I to the Fifth Assessment Report of the Intergovernmental Panel on Climate Change, edited by: Stocker, T. F., Qin, D., Plattner, G.-K., Tignor, M., Allen, S. K., Boschung, J., Nauels, A., Xia, Y., Bex, V., and Midgley, P. M., Cambridge University Press, Cambridge, United Kingdom and New York, NY, USA, 1535 pp., ISBN 978-1-107-05799-1, 2013.

IPCC: Climate Change 2021: The Physical Science Basis. Contribution of Working Group I to the Sixth Assessment Report of the Intergovernmental Panel on Climate Change, edited by: Masson-Delmotte, V., Zhai, P., Pirani, A., Connors, S. L., Péan, C., Berger, S., Caud, N., Chen, Y., Goldfarb, L., Gomis, M. I., Huang, M., Leitzell, K., Lonnoy, E., Matthews, J. B. R., Maycock, T. K., Waterfield, T., Yelekçi, O., Yu, R., and Zhou, B., Cambridge University Press, Cambridge, United Kingdom and New York, NY, USA, 2391 pp., doi:10.1017/9781009157896, 2021.

Jackson, L. C., Biastoch, A., Buckley, M. W., Desbruyères, D. G., Frajka-Williams, E., Moat, B., and Robson, J.: The evolution of the North Atlantic Meridional Overturning Circulation since 1980, Nat. Rev. Earth Environ., 3, 241–254, https://doi.org/10.1038/s43017-022-00263-2, 2022.

Jiang, L. Q., Feely, R. A., Carter, B. R., Greeley, D. J., Gledhill, D. K., and Arzayus, K. M.: Climatological distribution of aragonite saturation state in the global oceans, Global Biogeochem. Cy., 29, 1656–1673, https://doi.org/10.1002/2015GB005198, 2015.

Johnson, K. M., Wills, K. D., Butler, D. B., Johnson, W. K., and Wong, C. S.: Coulometric total carbon dioxide analysis for marine studies: maximizing the performance of an automated gas extraction system and coulometric detector, Mar. Chem., 44, 167–187, https://doi.org/10.1016/0304-4203(93)90201-X, 1993.

Josey, S. A., Hirschi, J. J. M., Sinha, B., Duchez, A., Grist, J. P., and Marsh, R.: The recent Atlantic cold anomaly: Causes, consequences, and related phenomena, Annu. Rev. Mar. Sci., 10, 475–501, https://doi.org/10.1146/annurev-marine-121916-063102, 2018.

Jung, T., Vitart, F., Ferranti, L., and Morcrette, J. J.: Origin and predictability of the extreme negative NAO winter of 2009/10, Geophys. Res. Lett., 38, L07803, https://doi.org/10.1029/2011GL047238, 2011.

Khatiwala, S., Tanhua, T., Mikaloff Fletcher, S., Gerber, M., Doney, S. C., Graven, H. D., Gruber, N., McKinley, G. A., Murata, A., Ríos, A. F., and Sabine, C. L.: Global Ocean storage of anthropogenic carbon, Biogeosciences, 10, 2169–2191, https://doi.org/10.5194/bg-10-2169-2013, 2013.

Kieke, D., Rhein, M., Stramma, L., Smethie, W. M., Bullister, J. L., and LeBel, D. A.: Changes in the pool of Labrador Sea Water in the subpolar North Atlantic, Geophys. Res. Lett., 34, L06601, https://doi.org/10.1029/2007GL029244, 2007.

Langdon, C., Takahashi, T., Sweeney, C., Chipman, D., and Atkinson, J.: Rate of an experimental coral reef responds to manipulations in the concentrations of both $CaCO_3$, Global Biogeochem. Cy., 14, 639–654, 2000.

Lauvset, S. K., Gruber, N., Landschützer, P., Olsen, A., and Tjiputra, J.: Trends and drivers in global surface ocean pH over the past 3 decades, Biogeosciences, 12, 1285–1298, https://doi.org/10.5194/bg-12-1285-2015, 2015.

Lazier, J., Hendry, R., Clarke, A., Yashayaev, I., and Rhines, P.: Convection and restratification in the Labrador Sea, 1990–2000, Deep-Sea Res. Pt. I, 49, 1819–1835, https://doi.org/10.1016/S0967-0637(02)00064-X, 2002.

Lee, K., Kim, T. W., Byrne, R. H., Millero, F. J., Feely, R. A., and Liu, Y. M.: The universal ratio of boron to chlorinity for the North

Pacific and North Atlantic oceans, Geochim. Cosmochim. Ac., 74, 1801–1811, https://doi.org/10.1016/j.gca.2009.12.027, 2010.

Leseurre, C., Lo Monaco, C., Reverdin, G., Metzl, N., Fin, J., Olafsdottir, S., and Racapé, V.: Ocean carbonate system variability in the North Atlantic Subpolar surface water (1993–2017), Biogeosciences, 17, 2553–2577, https://doi.org/10.5194/bg-17-2553-2020, 2020.

Lewis, E. and Wallace, D.: Program Developed for CO_2 System Calculations ORNL/CDIAC-105, Carbon Dioxide Information Analysis Centre [code], United State, https://doi.org/10.15485/1464255, 1998.

Lherminier, P., Mercier, H., Huck, T., Gourcuff, C., Perez, F. F., Morin, P., Sarafanov, A., and Falina, A.: The Atlantic Meridional Overturning Circulation and the subpolar gyre observed at the A25-OVIDE section in June 2002 and 2004, Deep-Sea Res. Pt. I, 57, 1374–1391, https://doi.org/10.1016/j.dsr.2010.05.004, 2010.

Lherminier, P., Perez, F. F., Branellec, P., Mercier, H., Velo, A., Messias, M. J., Castrillejo, M., Reverdin, G., Fontela, M., and Baurand, F.: GO-SHIP A25 – OVIDE 2018 Cruise data, SEANOE [data set], https://doi.org/10.17882/87394, 2022.

Lueker, T. J., Dickson, A. G., and Keeling, C. D.: Ocean $p\mathrm{CO}_2$ calculated from dissolved inorganic carbon, alkalinity, and equations for K_1 and K_2: Validation based on laboratory measurements of CO_2 in gas and seawater at equilibrium, Mar. Chem., 70, 105–119, https://doi.org/10.1016/S0304-4203(00)00022-0, 2000.

Maier-Reimer, E. and Hasselmann, K.: Transport and storage of CO_2 in the ocean: an inorganic ocean-circulation carbon cycle model, Clim. Dynam., 2, 63–90, 1987.

Maier, C., Hegeman, J., Weinbauer, M. G., and Gattuso, J. P.: Calcification of the cold-water coral Lophelia pertusa, under ambient and reduced pH, Biogeosciences, 6, 1671–1680, https://doi.org/10.5194/bg-6-1671-2009, 2009.

Marsh, R., de Cuevas, B. A., Coward, A. C., Bryden, H. L., and Álvarez, M.: Thermohaline circulation at three key sections in the North Atlantic over 1985–2002, Geophys. Res. Lett., 32, L23604, https://doi.org/10.1029/2004GL022281, 2005.

Matear, R. J. and Lenton, A.: Quantifying the impact of ocean acidification on our future climate, Biogeosciences, 11, 3965–3983, https://doi.org/10.5194/bg-11-3965-2014, 2014.

McCartney, M. S. and Talley, L. D.: The subpolar mode water of the North Atlantic Ocean, J. Phys. Oceanogr., 12, 1169–1188, 1982.

McGrath, T., Kivimäe, C., Tanhua, T., Cave, R. R., and McGovern, E.: Inorganic carbon and pH levels in the Rockall Trough 1991–2010, Deep-Sea Res. Pt. I, 68, 79–91, https://doi.org/10.1016/j.dsr.2012.05.011, 2012a.

McGrath, T., Nolan, G., and McGovern, E.: Chemical characteristics of water masses in the Rockall Trough, Deep-Sea Res. Pt. I, 61, 57–73, https://doi.org/10.1016/j.dsr.2011.11.007, 2012b.

McGrath, T., Kivimäe, C., McGovern, E., Cave, R. R., and Joyce, E.: Winter measurements of oceanic biogeochemical parameters in the Rockall Trough (2009–2012), Earth Syst. Sci. Data, 5, 375–383, https://doi.org/10.5194/essd-5-375-2013, 2013.

Mercier, H., Lherminier, P., Sarafanov, A., Gaillard, F., Daniault, N., Desbruyères, D., Falina, A., Ferron, B., Gourcuff, C., Huck, T., Thierry, V.: Variability of the meridional overturning circulation at the Greenland–Portugal OVIDE section from 1993 to 2010, Prog. Oceanogr., 132, 250–261, https://doi.org/10.1016/j.pocean.2013.11.001, 2015.

Messias, M. J., Watson, A. J., Johannessen, T., Oliver, K. I. C., Olsson, K. A., Fogelqvist, E., Olafsson, J., Bacon, S., Balle, J., Bergman, N., Budéus, G., Danielsen, M., Gascard, J. C., Jeansson, E., Olafsdottir, S. R., Simonsen, K., Tanhua, T., Van Scoy, K., and Ledwell, J. R.: The Greenland Sea tracer experiment 1996–2002: Horizontal mixing and transport of Greenland Sea Intermediate Water, Prog. Oceanogr., 78, 85–105, https://doi.org/10.1016/J.POCEAN.2007.06.005, 2008.

Millero, F. J., Zhang, J., Lee, K., and Campbell, D. M.: Titration alkalinity of seawater, Mar. Chem., 44, 153–165, 1993.

Mintrop, L., Pérez, F. F., González-Dávila, M., Santana-Casiano, J. M., and Körtzinger, A.: Alkalinity determination by potentiometry: Intercalibration using three different methods, Ciencias Mar., 26, 23–37, https://doi.org/10.7773/cm.v26i1.573, 2000.

Moss, R. H., Edmonds, J. A., Hibbard, K. A., Manning, M. R., Rose, S. K., Van Vuuren, D. P., Carter, T. R., Emori, S., Kainuma, M., Kram, T., Meehl, G. A., Mitchell, J. F. B., Nakicenovic, N., Riahi, K., Smith, S. J., Stouffer, R. J., Thomson, A. M., Weyant, J. P., and Wilbanks, T. J.: The next generation of scenarios for climate change research and assessment, Nature, 463, 747–756, https://doi.org/10.1038/nature08823, 2010.

Mucci, A.: The solubility of calcite and aragonite in seawater at various salinities, temperatures, and one atmosphere total pressure, Am. J. Sci., 283, 780–799, 1983.

Oceanology Group, IIM-CSIC: ′-CT0 CANT estimation method Matlab scripts, Oceanology Group, IIM-CSIC [code], http://oceano.iim.csic.es/co2group (last access: 9 December 2024), 2016.

Olafsson, J., Olafsdottir, S. R., Benoit-Cattin, A., Danielsen, M., Arnarson, T. S., and Takahashi, T.: Rate of Iceland Sea acidification from time series measurements, Biogeosciences, 6, 2661–2668, https://doi.org/10.5194/bg-6-2661-2009, 2009.

Olafsson, J., Olafsdottir, S. R., Benoit-Cattin, A., and Takahashi, T.: The Irminger Sea and the Iceland Sea time series measurements of seawater carbon and nutrient chemistry 1983–2008, Earth Syst. Sci. Data, 2, 99–104, https://doi.org/10.5194/essd-2-99-2010, 2010.

Orr, J. C., Fabry, V. J., Aumont, O., Bopp, L., Doney, S. C., Feely, R. A., Gnanadesikan, A., Gruber, N., Ishida, A., Joos, F., Key, R. M., Lindsay, K., Maier-Reimer, E., Matear, R., Monfray, P., Mouchet, A., Najjar, R. G., Plattner, G. K., Rodgers, K. B., Sabine, C. L., Sarmiento, J. L., Schlitzer, R., Slater, R. D., Totterdell, I. J., Weirig, M. F., Yamanaka, Y., and Yool, A.: Anthropogenic ocean acidification over the twenty-first century and its impact on calcifying organisms, Nature, 437, 681–686, https://doi.org/10.1038/nature, 2005.

Orr, J. C., Epitalon, J.-M., Dickson, A. G., and Gattuso, J.-P.: Routine uncertainty propagation for the marine carbon dioxide system, Mar. Chem., 207, 84–107, https://doi.org/10.1016/j.marchem.2018.10.006, 2018.

Ostle, C., Landschützer, P., Edwards, M., Johnson, M., Schmidtko, S., Schuster, U., Watson, A. J., and Robinson, C.: Multidecadal changes in biology influence the variability of the North Atlantic carbon sink, Environ. Res. Lett., 17, 114056, https://doi.org/10.1088/1748-9326/ac9ecf, 2022.

Pérez, F. F. and Fraga, F.: Association constant of fluoride and hydrogen ions in seawater, Mar. Chem., 21, 161–168, https://doi.org/10.1016/0304-4203(87)90036-3, 1987.

Pérez, F. F., Vázquez-Rodríguez, M., Louarn, E., Padín, X. A., Mercier, H., and Ríos, A. F.: Temporal variability of the anthropogenic CO_2 storage in the Irminger Sea, Biogeosciences, 5, 1669–1679, https://doi.org/10.5194/bg-5-1669-2008, 2008.

Pérez, F. F., Vázquez-Rodríguez, M., Mercier, H., Velo, A., Lherminier, P., and Ríos, A. F.: Trends of anthropogenic CO2 storage in North Atlantic water masses, Biogeosciences, 7, 1789–1807, https://doi.org/10.5194/bg-7-1789-2010, 2010.

Pérez, F. F., Mercier, H., Vázquez-Rodríguez, M., Lherminier, P., Velo, A., Pardo, P. C., Rosón, G., and Ríos, A. F.: Atlantic Ocean CO_2 uptake reduced by weakening of the meridional overturning circulation, Nat. Geosci., 6, 146–152, https://doi.org/10.1038/ngeo1680, 2013.

Pérez, F. F., Fontela, M., García-Ibáñez, M. I., Mercier, H., Velo, A., Lherminier, P., Zunino, P., De La Paz, M., Alonso-Pérez, F., Guallart, E. F., and Padin, X. A.: Meridional overturning circulation conveys fast acidification to the deep Atlantic Ocean, Nature, 554, 515–518, https://doi.org/10.1038/nature25493, 2018.

Pérez, F. F., Olafsson, J., Ólafsdóttir, S. R., Fontela, M., and Takahashi, T.: Contrasting drivers and trends of ocean acidification in the subarctic Atlantic, Sci. Rep., 11, 1–16, https://doi.org/10.1038/s41598-021-93324-3, 2021.

Pérez, F. F., Becker, M., Goris, N., Gehlen, M., Lopez-Mozos, M., Tjiputra, J., Olsen, A., Müller, J. D., Huertas, I. E., Chau, T. T. T., Cainzos, V., Velo, A., Benard, G., Hauck, J., Gruber, N., and Wanninkhof, R.: An assessment of CO_2 storage and sea-air fluxes for the Atlantic Ocean and Mediterranean Sea between 1985 and 2018, Global Biogeochem. Cy., 38, e2023GB007862, https://doi.org/10.1029/2023GB007862, 2024.

Pickart, R. S., Spall, M. A., Ribergaard, M. H., Moore, G. W. K., and Milliff, R. F.: Deep convection in the Irminger Sea forced by the Greenland tip jet, Nature, 424, 152–156, https://doi.org/10.1038/nature01729, 2003.

Piron, A., Thierry, V., Mercier, H., and Caniaux, G.: Gyre-scale deep convection in the subpolar North Atlantic Ocean during winter 2014–2015, Geophys. Res. Lett., 44, 1439–1447, https://doi.org/10.1002/2016GL071895, 2017.

Pollard, R. T., Griffiths, M. J., Cunningham, S. A., Read, J. F., Pérez, F. F., and Ríos, A. F.: Vivaldi 1991 – A study of the formation, circulation, and ventilation of Eastern North Atlantic Central Water, Prog. Oceanogr., 37, 167–172, https://doi.org/10.1016/S0079-6611(96)00008-0, 1996.

Pörtner, H. O., Langenbuch, M., and Reipschläger, A.: Biological Impact of Elevated Ocean CO_2 Concentrations: Lessons from Animal Physiology and Earth History, J. Oceanogr., 60, 705–718, 2004.

IPCC: IPCC Special Report on the Ocean and Cryosphere in a Changing Climate, edited by: Pörtner, H.-O., Roberts, D. C., Masson-Delmotte, V., Zhai, P., Tignor, M., Poloczanska, E., Mintenbeck, K., Alegría, A., Nicolai, M., Okem, A., Petzold, J., Rama, B., and Weyer, N. M., Cambridge University Press, Cambridge, UK and New York, NY, USA, 755 pp., https://doi.org/10.1017/9781009157964, 2019.

Ramette, R. W., Culberson, C. H., and Bates, R. G.: Acid-base properties of tris(hydroxymethyl) aminomethane (tris) buffers in seawater from 5 to 40 °C, Anal. Chem., 49, 867–870, https://doi.org/10.1021/ac50014a049, 1977.

Raven, J., Caldeira, K., Elderfield, H., Hoegh-Guldberg, O., Liss, P., Riebesell, U., Shepherd, J., Turley, C., and Watson, A. (Eds.): Ocean Acidification due to Increasing Atmospheric Carbon Dioxide, The Royal Society, ISBN 0 85403 617 2, 2005.

Read, J. F.: CONVEX-91: Water masses and circulation of the Northeast Atlantic subpolar gyre, Prog. Oceanogr., 48, 461–510, https://doi.org/10.1016/S0079-6611(01)00011-8, 2000.

Riebesell, U., Zondervan, I., Rost, B., Tortell, P. D., Zeebe, R. E., and Morel, F. M. M.: Reduced calcification of marine plankton in response to increased atmospheric CO_2, Nature, 407, 364–366, https://doi.org/10.1038/35030078, 2000.

Ríos, A. F., Resplandy, L., García-Ibáñez, M. I., Fajar, N. M., Velo, A., Padin, X. A., Wanninkhof, R., Steinfeldt, R., Rosón, G., Pérez, F. F., and Morel, F. M. M.: Decadal acidification in the water masses of the Atlantic Ocean, P. Natl. Acad. Sci. USA, 112, 9950–9955, https://doi.org/10.1073/pnas.1504613112, 2015.

Roberts, J. M., Wheeler, A. J., Freiwald, A., and Cairns, S.: Cold-Water Corals: The Biology and Geology of Deep-Sea Coral Habitats, Cambridge Univ. Press, https://doi.org/10.1017/CBO9780511581588, 2009.

Robson, J., Hodson, D., Hawkins, E., and Sutton, R.: Atlantic overturning in decline?, Nat. Geosci., 7, 2–3, https://doi.org/10.1038/ngeo2050, 2014.

Robson, J., Ortega, P., and Sutton, R.: A reversal of climatic trends in the North Atlantic since 2005, Nat. Geosci., 9, 513–517, https://doi.org/10.1038/ngeo2727, 2016.

Rodgers, K. B., Key, R. M., Gnanadesikan, A., Sarmiento, J. L., Aumont, O., Bopp, L., Doney, S. C., Dunne, J. R., Glover, D. M., Ishida, A., Ishii, M., Jacobson, A. R., Monaco, C. L., Maier-Reimer, E., Mercier, H., Metzl, N., Pérez, F. F., Rios, A. F., Wanninkhof, R., Wetzel, P., Winn, C. D., and Yamanaka, Y.: Using altimetry to help explain patchy changes in hydrographic carbon measurements, J. Geophys. Res.-Ocean., 114, 1–20, https://doi.org/10.1029/2008JC005183, 2009.

Sabine, C. L., Feely, R. A., Gruber, N., Key, R. M., Lee, K., Bullister, J. L., Wanninkhof, R., Wong, C. S., Wallace, D. W. R., Tilbrook, B., Millero, F. J., Peng, T. H., Kozyr, A., Ono, T., and Rios, A. F.: The oceanic sink for anthropogenic CO_2, Science, 305, 367–371, https://doi.org/10.1126/science.1097403, 2004.

Santana-Casiano, J. M., González-Dávila, M., Rueda, M.-J., Llinás, O., and González-Dávila, E.-F.: The interannual variability of oceanic CO_2 parameters in the northeast Atlantic subtropical gyre at the ESTOC site, Global Biogeochem. Cy., 21, GB1015, https://doi.org/10.1029/2006GB002788, 2007.

Santana-Casiano, J. M., González-Dávila, M., and Curbelo-Hernández, D.: Surface-to-bottom data of total alkalinity, total inorganic carbon, pH and dissolved oxygen in the subpolar North Atlantic along the CLIVAR 59.5N hydrographic section during 2009–2019, Zenodo [data set], https://doi.org/10.5281/zenodo.10276222, 2023.

Sarafanov, A., Mercier, H., Falina, A., and Sokov, A.: Cessation and partial reversal of deep water freshening in the northern North Atlantic: observation-based estimates and attribution, Tellus A, 62, 80–90, https://doi.org/10.1111/j.1600-0870.2009.00418.x, 2010.

Sarafanov, A., Falina, A., Mercier, H., Sokov, A., Lherminier, P., Gourcuff, C., Gladyshev, S., Gaillard, F., and Daniault, N.: Mean full-depth summer circulation and transports at the northern periphery of the Atlantic Ocean in the 2000s, J. Geophys. Res.-Ocean., 117, C01014, https://doi.org/10.1029/2011JC007572, 2012.

Sarafanov, A., Falina, A., Sokov, A., Zapotylko, V., and Gladyshev, S.: Ship-Based Monitoring of the Northern North Atlantic Ocean by the Shirshov Institute of Oceanology, The Main Results, in: The Ocean in Motion, edited by: Velarde, M., Tarakanov, R., and Marchenko, A., Springer Oceanography, Springer, Cham, https://doi.org/10.1007/978-3-319-71934-4_25, 2018.

Sarmiento, J. L., Orr, J. C., and Siegenthaler, U.: A perturbation simulation of CO_2 uptake in an ocean general circulation model, J. Geophys. Res.-Ocean., 97, 3621–3645, https://doi.org/10.1029/91JC02849, 1992.

Saunders, P. M.: Chapter 5.6 The dense northern overflows, Int. Geophys., 77, 401–417, https://doi.org/10.1016/S0074-6142(01)80131-5, 2001.

Sauzède, R., Bittig, H. C., Claustre, H., de Fommervault, O. P., Gattuso, J. P., Legendre, L., and Johnson, K. S.: Estimates of water-column nutrient concentrations and carbonate system parameters in the global ocean: A novel approach based on neural networks, Front. Mar. Sci., 4, 1–17, https://doi.org/10.3389/fmars.2017.00128, 2017.

Schlitzer, R.: Ocean Data View, https://odv.awi.de (last access: 9 December 2024), 2021.

Schmitz Jr., W. J. and McCartney, M. S.: On the north Atlantic circulation, Rev. Geophys., 31, 29–49, 1993.

Schott, F. A. and Brandt, P.: Circulation and deep water export of the subpolar North Atlantic during the 1990's, in: Ocean Circulation: Mechanisms and Impacts, edited by: Schmittner, A., Chiang, J. C. H., and Hemming, S. R., Geophysical Monograph Series, 173, AGU (American Geophysical Union), Washington, DC, 91–118, https://doi.org/10.1029/173GM08, 2007.

Sharp, J. D., Pierrot, D., Humphreys, M. P., Epitalon, J.-M., Orr, J. C., Lewis, E. R., and Wallace, D. W. R.: CO2SYSv3 for MATLAB (Version v3.2.1), Zenodo, https://doi.org/10.5281/zenodo.3950562, 2023.

Smeed, D. A., Josey, S. A., Beaulieu, C., Johns, W. E., Moat, B. I., Frajka-Williams, E., Rayner, D., Meinen, C. S., Baringer, M. O., Bryden, H. L., and McCarthy, G. D.: The North Atlantic Ocean Is in a State of Reduced Overturning, Geophys. Res. Lett., 45, 1527–1533, https://doi.org/10.1002/2017GL076350, 2018.

Steinfeldt, R., Rhein, M., Bullister, J. L., and Tanhua, T.: Inventory changes in anthropogenic carbon from 1997–2003 in the Atlantic Ocean between 20° S and 65° N, Global Biogeochem. Cy., 23, GB3010, https://doi.org/10.1029/2008GB003311, 2009.

Stramma, L., Kieke, D., Rhein, M., Schott, F., Yashayaev, I., and Koltermann, K. P.: Deep water changes at the western boundary of the subpolar North Atlantic during 1996 to 2001, Deep-Sea Res. Pt. I, 51, 1033–1056, https://doi.org/10.1016/J.DSR.2004.04.001, 2004.

Sutherland, D. A. and Pickart, R. S.: The East Greenland coastal current: Structure, variability, and forcing, Prog. Oceanogr., 78, 58–77, 2008.

Takahashi, T., Olafsson, J., Goddard, J. G., Chipman, D. W., and Sutherland, S. C.: Seasonal variation of CO_2 and nutrients in the high-latitude surface oceans: A comparative study, Global Biogeochem. Cy., 7, 843–878, https://doi.org/10.1029/93GB02263, 1993.

Takahashi, T., Sutherland, S.C., Wanninkhof, R., Sweeney, C., Feely, R. A., Chipman, D. W., Hales, B., Friederich, G., Chavez, F., Sabine, C., Watson, A., Bakker, D. C. E., Schuster, U., Metzl, N., Yoshikawa-Inoue, H., Ishii, M., Midorikawa, T., Nojiri, Y., Körtzinger, A., Steinhoff, T., Hoppema, M., Olafsson, J., Arnarson, T. S., Tilbrook, B., Johannessen, T., Olsen, A., Bellerby, R., Wong, C. S., Delille, B., Bates, N. R., and de Baar, H. J. W.: Climatological mean and decadal change in surface ocean pCO_2, and net sea-air CO_2 flux over the global oceans, Deep-Sea Res. Pt. II, 56, 554–577, https://doi.org/10.1016/j.dsr2.2008.12.009, 2009.

Tanhua, T., Körtzinger, A., Friis, K., Waugh, D. W., and Wallace, D. W. R.: An estimate of anthropogenic CO_2 inventory from decadal changes in oceanic carbon content, P. Natl. Acad. Sci. USA, 104, 3037–3042, https://doi.org/10.1073/pnas.0606574104, 2007.

Tesdal, J. E., Abernathey, R. P., Goes, J. I., Gordon, A. L., and Haine, T. W. N.: Salinity trends within the upper layers of the subpolar North Atlantic, J. Climate, 31, 2675–2698, https://doi.org/10.1175/JCLI-D-17-0532.1, 2018.

Thomas, H., Prowe, A. E. F., Lima, I. D., Doney, S. C., Wanninkhof, R., Greatbatch, R. J., Schuster, U., and Corbière, A.: Changes in the North Atlantic Oscillation influence CO_2 uptake in the North Atlantic over the past 2 decades, Global Biogeochem. Cy., 22, 1–13, https://doi.org/10.1029/2007GB003167, 2008.

Tjiputra, J. F., Olsen, A., Bopp, L., Lenton, A., Pfeil, B., Roy, T., Segschneider, J., Totterdell, I., and Heinze, C.: Long-term surface pCO_2 trends from observations and models, Tellus B, 66, 1–24, https://doi.org/10.3402/tellusb.v66.23083, 2014.

Touratier, F., Azouzi, L., and Goyet, C.: CFC-11, $\Delta^{14}C$ and ^{3}H tracers as a means to assess anthropogenic CO_2 concentrations in the ocean, Tellus B, 59, 318–325, https://doi.org/10.1111/j.1600-0889.2007.00247.x, 2007.

Tsuchiya, M., Talley, L. D., and McCartney, M. S.: An eastern Atlantic section from Iceland southward across the equator, Deep-Sea Res. Pt. A, 39, 1885–1917, https://doi.org/10.1016/0198-0149(92)90004-D, 1992.

Turley, C. M., Roberts, J. M., and Guinotte, J. M.: Corals in deep-water: will the unseen hand of ocean acidification destroy cold-water ecosystems?, Coral Reefs, 26, 445–448, https://doi.org/10.1007/s00338-007-0247-5, 2007.

Urban-Rich, J., Dagg, M., and Peterson, J.: Copepod grazing on phytoplankton in the Pacific sector of the Antarctic polar front, Deep-Sea Res. Pt. II, 48, 4223–4246, https://doi.org/10.1016/S0967-0645(01)00087-X, 2001.

Våge, K., Pickart, R. S., Thierry, V., Reverdin, G., Lee, C. M., Petrie, B., Agnew, T. A., Wong, A., and Ribergaard, M. H.: Surprising return of deep convection to the subpolar North Atlantic Ocean in winter 2007–2008, Nat. Geosci., 2, 67–72, https://doi.org/10.1038/ngeo382, 2009.

van Aken, H. M. and Becker, G.: Hydrography and through-flow in the north-eastern North Atlantic Ocean: the NANSEN project, Prog. Oceanogr., 38, 297–346, https://doi.org/10.1016/S0079-6611(97)00005-0, 1996.

van Aken, H. M. and De Boer, C. J.: On the synoptic hydrography of intermediate and deep water masses in the Iceland Basin, Deep-Sea Res. Pt. I, 42, 165–189, 1995.

van Heuven, S., Pierrot, D., Rae, J. W. B., Lewis, E., and Wallace, D. W. R.: MATLAB Program Developed for CO2 System Calculations, ORNL/CDIAC-105b, Carbon Dioxide Information Analysis Center, Oak Ridge National Laboratory, U.S. Department of Energy, Oak Ridge, Tennessee, 2011.

Van Vuuren, D. P., Edmonds, J., Kainuma, M., Riahi, K., Thomson, A., Hibbard, K., Hurtt, G. C., Kram, T., Krey, V., Lamarque, J.-F., Masui, T., Meinshausen, M., Nakicenovic, N., Smith, S. J., and Rose, S. K.: The representative concentration pathways: an overview, Climatic Change, 109, 5–31, https://doi.org/10.1007/s10584-011-0148-z, 2011.

Vázquez-Rodríguez, M., Touratier, F., Monaco, C. L., Waugh, D. W., Padin, X. A., Bellerby, R. G. J., Goyet, C., Metzl, N., Ríos, A. F., and Pérez, F. F.: Anthropogenic carbon distributions in the Atlantic Ocean: Data-based estimates from the Arctic to the Antarctic, Biogeosciences, 6, 439–451, https://doi.org/10.5194/bg-6-439-2009, 2009.

Vázquez-Rodríguez, M., Padin, X. A., Pardo, P. C., Ríos, A. F., and Pérez, F. F.: The subsurface layer reference to calculate preformed alkalinity and air-sea CO_2 disequilibrium in the Atlantic Ocean, J. Mar. Syst., 94, 52–63, https://doi.org/10.1016/j.jmarsys.2011.10.008, 2012a.

Vázquez-Rodríguez, M., Pérez, F. F., Velo, A., Ríos, A. F., and Mercier, H.: Observed acidification trends in North Atlantic water masses, Biogeosciences, 9, 5217–5230, https://doi.org/10.5194/bg-9-5217-2012, 2012b.

Wallace, D. W.: Storage and transport of excess CO_2 in the oceans: The JGOFS/WOCE global CO_2 survey, Int. Geophys., 77, 489–521, https://doi.org/10.1016/S0074-6142(01)80136-4, 2001.

Watson, A. J., Schuster, U., Bakker, D. C. E., Bates, N. R., Corbière, A., González-Davila, M., Friedrich, T., Hauck, J., Heinze, C., Johannessen, T., Körtzinger, A., Metzl, N., Olafsson, J., Olsen, A., Oschlies, A., Padin, X. A., Santana-Casiano, J. M., Steinhoff, T., Telszewski, M., Rios, A. F., Wallace, D. W. R., and Wanninkhof, R.: Tracking the variable North Atlantic sink for atmospheric CO_2, Science, 326, 1391–1393, https://doi.org/10.1126/science.1177394, 2009.

Winkler, L. W.: Die bestimmung des im wasser gelösten sauerstoffes, Ber. Dtsch. Chem. Ges., 21, 2843–2854, 1888.

Xu, X., Hurlburt, H. E., Zantopp, R., Fischer, J., and Hogan, P. J.: On the currents and transports connected with the Atlantic meridional overturning circulation in the subpolar North Atlantic, J. Geophys. Res., 118, 502–516, https://doi.org/10.1002/jgrc.20065, 2013.

Yashayaev, I.: Hydrographic changes in the Labrador Sea, 1960–2005, Prog. Oceanogr., 73, 242–276, https://doi.org/10.1016/j.pocean.2007.04.015, 2007.

Yashayaev, I. and Dickson, B.: Transformation and Fate of Overflows in the Northern North Atlantic, in: Arctic–Subarctic Ocean Fluxes, edited by: Dickson, R. R., Meincke, J., and Rhines, P., Springer, Dordrecht, https://doi.org/10.1007/978-1-4020-6774-7_22, 2008.

Yashayaev, I., Holliday, N. P., Bersch, M., and van Aken, H. M.: The history of the Labrador Sea Water: Production, spreading, transformation and loss, in: Arctic-Subarctic Ocean Fluxes, edited by: Dickson, R. R., Meincke, J., and Rhines, P., Berlin, Springer, 569–612, 736 pp., ISBN: 978-1-4020-6773-0, 2008.

Yashayaev, I., Lazier, J., and Clarke, R.: Temperature and salinity in the central Labrador Sea during the 1990s and in the context of the longer-term change, ICES MSS Vol. 219, https://doi.org/10.17895/ices.pub.19271729.v1, 2003.